

RESEARCH ARTICLE

WILEY

FAST.Farm development and validation of structural load prediction against large eddy simulations

Kelsey Shaler  | Jason Jonkman

National Renewable Energy Laboratory,
Golden, Colorado, USA

Correspondence

Kelsey Shaler, National Renewable Energy
Laboratory, Golden, CO, USA.
Email: kelsey.shaler@nrel.gov

Funding information

Wind Energy Technologies Office, Grant/
Award Number: Contract No. DE-
AC36-08GO28308

Abstract

FAST.Farm is a mid-fidelity engineering tool developed by the National Renewable Energy Laboratory targeted at accurately and efficiently predicting wind turbine power production and structural loading in wind farm settings, including wake interactions between turbines. FAST.Farm is based on several principles of the dynamic wake meandering (DWM) model, but also addresses limitations of previous DWM implementations. Previous FAST.Farm studies have shown the similarities and differences between FAST.Farm and large eddy simulations for rigid turbine cases. The objective of this work is to quantify the ability of FAST.Farm to accurately predict turbine structural response in a small wind farm. This is done by comparing FAST.Farm structural response to SOWFA-OpenFAST results for three laterally-aligned turbines. The purpose of this study is to characterize the similarities and differences between FAST.Farm and a higher fidelity model for predicting turbine structural response in a wind farm for differing atmospheric inflows. Strong statistical agreement was found between FAST.Farm and SOWFA-OpenFAST structural response for the non-waked upstream turbine, and good agreement was found for the downstream turbines for most structural quantities. Higher differences were seen for downstream turbines with low ambient turbulence intensity or yawed turbines, suggesting areas for FAST.Farm wake dynamics modeling improvements. For all cases and turbines, small statistical differences were seen between blade deflections and bending moments, with larger differences for tower-top and tower-base bending moments. Overall, the results establish confidence for applying FAST.Farm to wind farm power and loads analyses and identify areas where further model validations and model improvements should be targeted.

KEYWORDS

FAST.Farm, SOWFA, turbine structural loads, turbine wakes, wind farm

This is an open access article under the terms of the Creative Commons Attribution-NonCommercial-NoDerivs License, which permits use and distribution in any medium, provided the original work is properly cited, the use is non-commercial and no modifications or adaptations are made.

Published 2020. This article is a U.S. Government work and is in the public domain in the USA. Wind Energy published by John Wiley & Sons Ltd

1 | INTRODUCTION

In the context of wind farm design and optimization, it is crucial to be able to perform thousands of wind farm-scale simulations expediently. This requires a model that is able to accurately predict dynamic turbine performance while remaining computationally inexpensive. Low-fidelity models, such as the FLOW Redirection and Induction in Steady state (FLORIS) model,¹ can compute full wind farm mean power on the order of seconds and are often used for optimization studies.² However, such steady-state models cannot be used for analysis of structural loads. Such analysis requires a dynamic turbine response and is a critical step in wind farm design. High-fidelity modeling, such as the large eddy simulation (LES) model known as Simulator fOr Wind Farm Applications (SOWFA), can be used to capture dynamic turbine performance and loads by directly resolving the large, energy-containing scales of turbulence and wake dynamics.³ However, such methods have a high computational expense and are intractable for use in the design process. FAST.Farm is a new mid-fidelity engineering tool developed by the National Renewable Energy Laboratory (NREL) for use in the wind farm design process. This tool aims to model the wake dynamics of wind farms for the purpose of accurately and efficiently predicting wind turbine power production and structural loading, including wake interactions between turbines in the farm based on advancements to the dynamic wake meandering (DWM) model.⁴

In past work, FAST.Farm was verified against results from SOWFA. Results were compared for laterally aligned three-turbine configurations with different inflow and control conditions using turbulent ambient wind data generated by an LES precursor and synthetic inflow.^{5,6} These studies showed that FAST.Farm did reasonably well at capturing the statistical distributions of turbine power and thrust with lower computational expense. No quantitative analysis of percent differences between turbine response for differing computational methods was included. Additionally, horizontal and vertical wake meandering, as well as wake deficit advection, evolution, and merging, were captured reasonably well by FAST.Farm. Although these results are promising, the turbines were modeled rigidly and the studies did not consider wind turbine structural loads other than thrust and torque. Another study compared FAST.Farm turbine response with multiturbine measurements from a subset of a full-scale wind farm.⁷ FAST.Farm predictions of turbine generator power, rotor speed, and blade pitch for five-turbine simulations are compared with supervisory control and data acquisition (SCADA) results. Results revealed that FAST.Farm generator power mean and standard deviation results reasonably match measured data for upstream and downstream turbines, as well as the mean rotor speed and blade pitch above rated wind speeds. However, FAST.Farm generally underpredicted the mean rotor speed and overpredicted the mean blade pitch below rated operation. These errors were likely related to inaccuracies in the generic controller simulated. Despite controller differences, FAST.Farm predicted the same overall relative rotor power trends for all waked turbines at all wind speeds. The only other validation study to compare FAST.Farm simulations to measurements was the Scaled Wind Farm Technology (SWiFT) benchmark study.⁸ Results showed that underperforming aspects of the simulated wakes were primarily a result of inaccuracies in the inflow and not related to wake modeling itself. FAST.Farm has also been used to study the effects of atmospheric lateral coherence and wake meandering on downstream turbine performance⁶ and fatigue loads.^{9,10} These studies found that wake meandering has a large effect on downstream turbine power production and fatigue loads, making this an important physical feature to accurately model.

The promising capabilities of FAST.Farm for predicting turbine performance in a wind farm have been established.⁵⁻⁷ However, no studies have quantified the ability of FAST.Farm to accurately predict turbine structural response in a small wind farm. The objective of this work is to perform such a study. This is done by comparing FAST.Farm structural response with coupled SOWFA-OpenFAST results for three laterally aligned turbines. The purpose of this study is to characterize the similarities and differences between FAST.Farm and a higher fidelity model for predicting turbine structural response in a wind farm for differing atmospheric inflows.

2 | APPROACH AND METHODS

This section provides an overview of FAST.Farm with a focus on recent modeling improvements, followed by a description of all modeling cases used in this study.

2.1 | Overview of FAST.Farm

FAST.Farm is a multiphysics engineering tool that accounts for wake interaction effects on turbine performance and structural loading in wind farm applications. FAST.Farm is an extension of the NREL software OpenFAST, which solves the aero-hydro-servo-elasto dynamics of individual turbines. FAST.Farm extends this analysis to include wake deficits, advection, deflection, meandering, and merging for wind farms. FAST.Farm is based on the DWM model¹¹ but expands on it to address many limitations of past DWM implementations. The development and mathematical details of FAST.Farm were originally presented in Jonkman et al.⁴ This section summarizes the key principles of how the model works, using key mathematical expressions to aid in clarity, where relevant.

The main idea behind the DWM model is to capture key wake features pertinent to accurate prediction of wind farm power performance and wind turbine structural loads, including the wake deficit (important for performance) and wake meandering (important for loads). Although

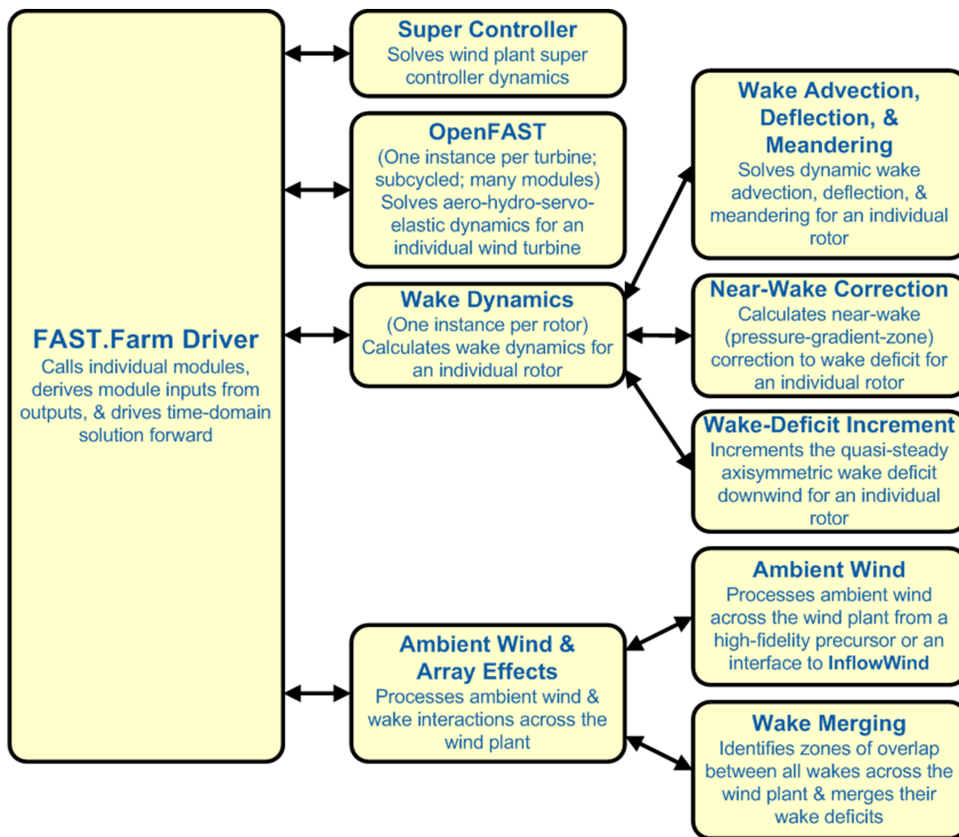


FIGURE 1 FAST.Farm submodel hierarchy [Colour figure can be viewed at wileyonlinelibrary.com]

fundamental laws of physics are applied, appropriate simplifications have been made to minimize the computational expense, and high-fidelity modeling solutions are used to inform and calibrate the submodels.

FAST.Farm is composed of multiple submodels, each representing different physics domains of the wind farm. FAST.Farm is implemented as open-source software that follows the programming requirements of the FAST modularization framework,¹² whereby the submodels are implemented as modules interconnected through a driver code. The submodel hierarchy of FAST.Farm is illustrated in Figure 1. Wake advection, deflection, and meandering; near-wake correction; and wake deficit increment are submodels of the wake dynamics module. Ambient wind and wake merging are submodels of the ambient wind and array effects module. Combined with the super controller* and OpenFAST modules, FAST.Farm has four modules and one driver. There are multiple instances of the OpenFAST and wake dynamics modules—one instance for each wind turbine. Each submodel/module is described in the following subsections.

2.1.1 | FAST.Farm driver

The FAST.Farm driver couples individual modules together and drives the overall time-domain solution forward. After initialization, within each time step, the states of each module are updated to the next time step, time is incremented, and the module outputs are calculated and transferred as inputs to other modules. The FAST.Farm time step is consistent with the timescales of wake dynamics (e.g., $\leq \mathcal{O}$, in seconds, depending on mean wind speeds).

FAST.Farm can be compiled and run in serial or parallel mode. In parallel mode, each instance of OpenFAST can be run on separate threads while the ambient wind is being read on another thread. Thus, simulations would ideally employ at least one more processor than the number of wind turbines in the wind farm. Furthermore, the calculations within the ambient wind and array effects module are parallelized into separate threads. The size of the wind farm and number of wind turbines is limited only by the available RAM.

The OpenFAST module is the computationally slowest of the FAST.Farm modules because of the small timescales and complex, nonlinear physics involved. Additionally, the output calculation of the ambient wind and array effects module is the only major calculation that cannot be solved parallel to OpenFAST. Therefore, the parallelized FAST.Farm solution at its fastest may execute slightly slower than stand-alone OpenFAST

*The super controller module of FAST.Farm allows wind farm-wide control logic to be implemented, including sending and receiving commands from the individual turbine controllers in OpenFAST. Further details are not included because they were not used in this work.

simulations. This makes FAST.Farm computationally inexpensive enough to run the many simulations necessary for wind turbine/farm design and analysis.

2.1.2 | OpenFAST

OpenFAST is used to model the dynamics (loads and motions) of distinct turbines in the wind farm, capturing the environmental excitation (e.g., wind inflow) and coupled system response (e.g., the rotor, drivetrain, nacelle, tower, controller).[†] OpenFAST itself is an interconnection of various modules, each corresponding to different physical domains of the coupled aero-hydro-servo-elastic solution.

At initialization, the number of wind turbines and their origin in the global inertial-frame coordinate system are specified. At each FAST.Farm time step, OpenFAST receives as input the commands from the super controller and the disturbed wind (ambient wind plus wakes of neighboring turbines) across a high resolution in both time and space wind domain. This ensures that the individual turbine loads and response calculated by OpenFAST are accurately driven by flow through the wind farm, including wake and array effects. OpenFAST outputs the rotor position, orientation, and radially dependent thrust coefficient. For accuracy and numerical stability reasons, the OpenFAST time step is typically much smaller than that required of FAST.Farm, resulting in OpenFAST being subcycled within the FAST.Farm solution.

2.1.3 | Wake dynamics

The wake dynamics module of FAST.Farm calculates the wake evolution for an individual rotor, including wake advection, deflection, and meandering; a near-wake correction, which accounts for pressure gradient zone effects on the wake deficit; and a wake deficit increment, which advances the quasi-steady-state axisymmetric wake deficit nominally downwind.

The wake dynamics calculations involve many user-specified parameters that may depend, for example, on turbine operation or atmospheric conditions that can be calibrated to better match experimental data or high-fidelity simulations. Default values have been derived for each calibrated parameter based on SOWFA simulations,¹³ but these can be overwritten by the user of FAST.Farm.

The wake deficit evolution is solved in discrete time on an axisymmetric finite-difference grid consisting of a fixed number of wake planes, each with a fixed radial grid of nodes. Because the wake deficit is assumed to be axisymmetric, the radial finite-difference grid can be considered a plane. A wake plane can be thought of as a cross section of the wake, wherein the wake deficit is calculated.

At each FAST.Farm time step, the wake dynamics module uses as input the rotor position, orientation, and radially dependent thrust distribution for an individual rotor, as well as the advection, deflection, and meandering velocity of the wake planes for the rotor, the rotor disk-averaged ambient wind speed normal to the disk, and the ambient turbulence intensity (TI) of the wind at the rotor. The wake dynamics module computes several outputs needed for the calculation of disturbed wind in the ambient wind and array effects module, including the positions and orientations of the wake planes and the axial and radial wake velocity deficits at the wake planes, distributed radially.

Wake advection, deflection, and meandering

By simple extensions to the passive tracer solution for transverse (horizontal and vertical) wake meandering, the wake dynamics solution in FAST.Farm is extended to account for wake deflection and wake advection, among other physical improvements, such as

1. calculating the wake plane velocities by spatially averaging the disturbed wind instead of the ambient wind;
2. orienting the wake planes with the rotor centerline instead of the wind direction; and
3. low-pass time filtering the local conditions at the rotor, as input to the wake dynamics module, to account for transients in inflow, turbine control, and/or turbine motion instead of considering time-averaged conditions.

With these extensions, the passive tracer solution enables

4. the wake centerline to deflect based on inflow skew, because in skewed inflow, the wake deficit normal to the disk introduces a velocity component that is not parallel to the ambient flow;
5. the wake to accelerate from near wake to far wake, because the wake deficits are stronger in the near wake and weaken downwind;
6. the wake deficit evolution to change based on conditions at the rotor, because low-pass time-filtered conditions are used instead of time averaging;
7. the wake to meander axially[‡] in addition to transversely, because local axial winds are considered; and
8. the wake shape to be elliptical instead of circular looking downwind when incoming flow is not normal to the rotor plane.

[†]OpenFAST also supports functionality for offshore wind turbines, not discussed here.

[‡]Wake planes may pulsate axially as they convect downstream, differentiating axial meandering from wake propagation.

For Item 6 above, low-pass time filtering is important because the wake reacts slowly to changes in local conditions at the rotor and because the wake evolution is treated in a quasi-steady-state fashion. Further details on the low-pass time filtering and calculations of wake plane orientations and positions can be found in the FAST.Farm User's Guide and Theory Manual.¹⁴

Near-wake correction

The near-wake correction submodel of the wake dynamics module computes the axial and radial wake velocity deficits at the rotor disk, as an inlet boundary condition for the wake deficit evolution submodel. To improve the accuracy of the far-wake solution, the near-wake correction accounts for the drop in wind speed and radial expansion of the wake in the pressure gradient zone behind the rotor that is not otherwise accounted for in the solution for the wake deficit evolution. For clarity, the equations in this section are expressed using continuous variables; however, within FAST.Farm, the equations are solved discretely on an axisymmetric finite-difference grid.

The states and outputs associated with the axial and radial wake velocity deficits, distributed radially, $V_{x_{np}}^{\text{Wake}}(r)$ and $V_{r_{np}}^{\text{Wake}}(r)$, respectively, are derived at the rotor disk ($n_p = 0$) from the axial induction at the rotor disk, distributed radially, $a(r)$, and the low-pass time-filtered rotor disk-averaged relative wind speed (ambient plus wakes of neighboring turbines plus turbine motion), normal to the disk, $\text{Filt} \bar{V}_x^{\text{Rel}}$, using Equation (1).

$$V_{x_{np}}^{\text{Wake}}(r^{\text{Plane}}) \Big|_{n_p=0} = -\text{Filt} \bar{V}_x^{\text{Rel}} C_{\text{NearWake}} a(r) \quad (1)$$

$$r^{\text{Plane}} = \sqrt{2 \int_0^r \frac{1-a(r')}{1-C_{\text{NearWake}} a(r')} r' dr'} \quad (2)$$

Here, r^{Plane} is the radial expansion of the wake associated with r ; r' is a dummy variable of r ; and C_{NearWake} is a user-specified parameter greater than unity, which determines how far the wind speed drops and the wake expands radially in the pressure gradient zone before recovering in the far wake.⁸

The right-hand side of Equation (1) represents the axial-induced velocity at the end of the pressure gradient zone; the negative sign appears because the axial wake deficit is in the opposite direction of the freestream axial wind. The radial expansion of the wake in the left-hand side of Equation (1) results from the application of the conservation of mass within an incremental annulus in the pressure gradient zone.

Because the near-wake correction is applied directly at the rotor disk, the solution to the wake deficit evolution for downwind distances within the first few diameters of the rotor (i.e., in the near wake) is not expected to be accurate; as a result, modifications to FAST.Farm would be needed to accurately model closely spaced wind farms.

Wake deficit increment

As with most DWM implementations, FAST.Farm models the wake deficit evolution via the thin shear layer approximation of the Reynolds-averaged Navier–Stokes equations under quasi-steady-state conditions in axisymmetric coordinates, with turbulence closure captured by using an eddy viscosity formulation.¹⁵ The thin shear layer approximation drops the pressure term and assumes that the velocity gradients are larger in the radial direction than in the axial direction. With these simplifications, analytical expressions for the conservation of momentum (Equation 3) and conservation of mass (continuity, Equation 4) are as follows:

$$V_x \frac{\partial V_x}{\partial x} + V_r \frac{\partial V_x}{\partial r} = \frac{1}{r} \frac{\partial}{\partial r} \left(r \nu_T \frac{\partial V_x}{\partial r} \right) \quad (3)$$

$$\frac{\partial V_x}{\partial x} + \frac{1}{r} \frac{\partial}{\partial r} (r V_r) = 0 \quad (4)$$

where V_x and V_r are the axial and radial velocities in the axisymmetric coordinate system, respectively, and ν_T is the eddy viscosity (all dependent on x and r , i.e., the downwind distance and radius in the axisymmetric coordinate system). The equations in this section are expressed using continuous variables, but within FAST.Farm, the equations are solved discretely on an axisymmetric finite-difference grid consisting of a fixed number of wake planes.

The axial and radial velocities are related to the low-pass time-filtered rotor disk-averaged ambient wind speed, normal to the disk, $\text{Filt} \bar{V}_x^{\text{Wind}}$, and the states and outputs are associated with the radially distributed axial and radial wake velocity deficits, $V_x^{\text{Wake}}(x, r)$ and $V_r^{\text{Wake}}(x, r)$, respectively, by Equations (5) and (6). $V_x^{\text{Wake}}(x, r)$ and $V_r^{\text{Wake}}(x, r)$ can be thought of as the change in wind velocity in the wake relative to freestream; therefore, $V_x^{\text{Wake}}(x, r)$ usually has a negative value.

⁸A value of $C_{\text{NearWake}} = 2$ is expected from first principles, but C_{NearWake} can be calibrated to better match the far wake to known solutions.¹³

$$V_x(x, r) = \text{Filt} \bar{V}_x^{\text{Wind}} + V_x^{\text{Wake}}(x, r) \quad (5)$$

$$V_r(x, r) = V_r^{\text{Wake}}(x, r) \quad (6)$$

The momentum and continuity equations are solved numerically in the wake deficit increment submodel of the wake dynamics module using a second-order accurate finite-difference method following the implicit Crank–Nicolson method.¹⁶ For each wake plane downstream of the rotor, $V_{x_{n_p}}^{\text{Wake}}(r)[n+1]$ can be solved via a linear tridiagonal matrix system of equations in terms of known solutions of $V_{x_{n_p-1}}^{\text{Wake}}(r)[n]$, $V_{r_{n_p-1}}^{\text{Wake}}(r)[n]$, and other previously calculated states (e.g., $\text{Filt} \bar{V}_{x_{n_p-1}}^{\text{Wind}}[n]$), where n is the time step and n_p is the wake plane. The finite-difference scheme used for the continuity equation is also based on a second-order accurate scheme, but different from that used for the momentum equation. The end result is that for each wake plane downstream of the rotor, $V_{r_{n_p}}^{\text{Wake}}[n+1]$ can be solved explicitly and sequentially from known solutions of $V_{x_{n_p}}^{\text{Wake}}(r)[n+1]$ (from the solution of the momentum equation), $V_{x_{n_p}}^{\text{Wake}}(r)[n]$, and $V_{r_{n_p, n_p-1}}^{\text{Wake}}[n+1]$. Note that the radial wake velocity deficit at the centerline of the axisymmetric coordinate system ($n_r = 0$) is always zero, $V_{r_{n_p}}^{\text{Wake}}(r)|_{r=0}$.

Several variations of the eddy viscosity formulation have been used in prior implementations of DWM. The eddy viscosity formulation currently implemented within FAST.Farm is given by Equation (7),

$$\begin{aligned} \nu_T(x, r) = & F_{\nu, \text{Amb}}(x) k_{\nu, \text{Amb}} \text{Filt} TI_{\text{Amb}} \text{Filt} \bar{V}_x^{\text{Wind}} R \\ & + F_{\nu, \text{Shr}}(x) k_{\nu, \text{Shr}} \text{MAX} \left[\left(\frac{D^{\text{Wake}}(x)}{2} \right)^2 \left| \frac{\partial V_x}{\partial r}(x, r) \right|, \frac{D^{\text{Wake}}(x)}{2} \text{MIN}_{|r} \{ V_x(x, r) \} \right] \end{aligned} \quad (7)$$

where $F_{\nu, \text{Amb}}(x)$ is the filter function associated with ambient turbulence; $F_{\nu, \text{Shr}}(x)$ is the filter function associated with the wake shear layer; $k_{\nu, \text{Amb}}$ is the user-specified calibration parameter weighting the influence of ambient turbulence on the eddy viscosity; $k_{\nu, \text{Shr}}$ is the user-specified calibration parameter weighting the influence of the wake shear layer on the eddy viscosity; $\text{Filt} TI_{\text{Amb}}$ is a low-pass time-filtered ambient TI; R is the rotor radius; $\frac{D^{\text{Wake}}}{2}$ is a wake half-width; $\left| \frac{\partial V_x}{\partial r} \right|$ is the absolute value of the radial gradient of the axial velocity; and $\text{MIN}_{|r} \{ V_x(x, r) \}$ is the minimum value of V_x along the radius for a given downstream distance.

The filter functions currently implemented within FAST.Farm are based on user-specified calibration parameters. Although not matching any specific eddy viscosity formulation found in prior implementations of DWM, the chosen implementation within FAST.Farm is simple to apply and inherently tailorable, allowing the user to properly calibrate the wake evolution to known solutions. The eddy viscosity formulation expresses the influence of the ambient turbulence (first term on the right-hand side) and wake shear layer (second term) on the turbulent stresses in the wake. The dependence of the eddy viscosity on x and r is explicitly given in Equation (7) to make it clear which terms depend on the downwind distance and/or radius. The first term on the right-hand side of Equation (7) is similar to that given by Madsen et al.,¹⁷ with a characteristic length taken to be the rotor radius. The second term is similar to that given by Keck et al.,¹⁸ but without consideration of atmospheric shear, which is considered by the ambient wind and array effects module in the definition of ambient turbulence. In this second term, the characteristic length is taken to be the wake half-width and the $\text{MAX}()$ operator is used to denote the maximum of the two wake shear layer methods. The second shear layer method is needed to avoid underpredicting the turbulent stresses from the first method at radii where the radial gradient of the axial velocity approaches zero.

2.1.4 | Ambient wind and array effects

The ambient wind and array effects module of FAST.Farm processes ambient wind and wake interactions across the wind farm, including the ambient wind submodel, which processes ambient wind across the wind farm, and the wake-merging submodel, which identifies zones of overlap between all wakes across the wind farm and merges their wake deficits.

The calculations in the ambient wind array effects module use wake volumes, which are volumes formed by a (possibly curved) cylinder starting at a wake plane and extending to the next adjacent wake plane along a line connecting the centers of the two wake planes. If the adjacent wake planes (top and bottom of the cylinder) are not parallel (e.g., for transient simulations involving variations in nacelle yaw angle), the centerline will be curved. Figure 2 illustrates some of these concepts. The calculations in the ambient wind and array effects module also require looping through all wind data points, turbines, and wake planes. These loops are sped up in the parallel mode of FAST.Farm by implementation of OpenMP parallelization. The module uses as input the positions, orientations, and wake deficits for each wake plane as computed by the wake dynamics module for each individual wind turbine and computes the disturbed wind needed for the calculation of turbine response in OpenFAST for each individual wind turbine, as well as the velocity of each wake plane and the ambient inflow and TI at the rotor needed for the calculation of wake dynamics for each individual wind turbine.

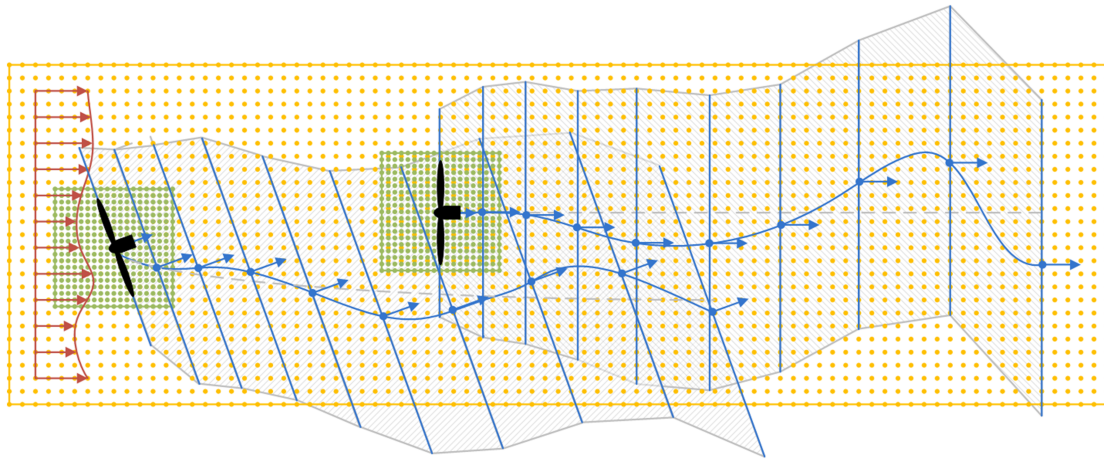


FIGURE 2 Wake planes, wake volumes, and zones of wake overlap for a two-turbine wind farm, with the upwind turbine yawed. The yellow points represent the low-resolution wind domain, and the green points represent the high-resolution wind domains around each turbine. The blue points and arrows represent the centers and orientations of the wake planes, respectively, with the wake planes identified by the blue lines normal to their orientations. The gray dashed lines represent the mean trajectory of the wake, and the blue curves represent an instantaneous (meandered) trajectory. The wake volumes associated with the upwind turbine are represented by the upward hatch patterns, the wake volumes associated with the downwind turbine are represented by the downward hatch patterns, and the zones of wake that overlap are represented by the crosshatch patterns. For clarity of the illustration, the instantaneous wake trajectory is shown as a smooth curve, but will be modeled as piece-wise linear between wake planes when adjacent wake planes are parallel. The wake planes and volumes are illustrated with a diameter equal to twice the wake diameter, but the local diameter depends on the calculation. As illustrated, a wake plane or volume may extend beyond the boundaries of the low-resolution domain of ambient wind data [Colour figure can be viewed at wileyonlinelibrary.com]

Ambient wind

FAST.Farm can use several types of ambient wind data, including uniform wind, discrete/deterministic wind events, or synthetically generated turbulent wind data.[¶] FAST.Farm can also use ambient wind generated by a high-fidelity precursor simulation, such as a SOWFA-generated atmospheric boundary layer precursor.^{20#} Comparison of FAST.Farm results for varying inflow techniques is detailed in Shaler et al.⁶

FAST.Farm requires ambient wind to be available in two different resolutions from overlapping domains. Because wind will be spatially averaged across wake planes within the ambient wind and array effects module, FAST.Farm needs a low-resolution wind domain throughout the wind farm. This domain is a structured three-dimensional (3D) grid of wind data points that will likely, but does not have to, be coarser in time and space than the high-resolution domain around the turbine. The spatial resolution of the low-resolution domain should be sufficient so that the spatial averaging is accurate. While the spatial resolution could be as fine as the high-resolution domain, that will unnecessarily increase computational expense. The time step of the low-resolution domain dictates the time step of the FAST.Farm driver and all FAST.Farm modules and should therefore be consistent with the timescales of wake dynamics. For accurate load calculations by OpenFAST, FAST.Farm also needs high-resolution wind domains (in both space and time) around each wind turbine and encompassing any turbine displacement. The spatial and time resolution of each high-resolution domain should be sufficient for accurate aerodynamic load calculations. Guidance on proper spatial and temporal discretizations is provided in Shaler et al.²¹ Care should be taken to ensure consistency in flow between the low-resolution and high-resolution domains. Guidance on ambient inflow generation is given in the FAST.Farm User's Guide and Theory Manual.¹⁴

After the ambient wind is processed at a given time step, the ambient wind submodel computes the rotor disk-averaged ambient wind speed normal to the disk, \bar{V}_x^{Wind} , for each turbine. \bar{V}_x^{Wind} is calculated as the uniform spatial average of the ambient wind velocity on the wake plane at the rotor disk ($n_p = 0$) projected along the low-pass time-filtered rotor centerline, expressed in Equation (8).

$$\bar{V}_x^{\text{Wind}} = \left\{ (\hat{x}_{n_p})^T \frac{1}{N_{n_p}} \sum_{n=1}^{N_{n_p}} \bar{V}_{\text{Amb}_n} \right\} \Big|_{n_p=0} \quad (8)$$

Here, \bar{V}_{Amb} is the ambient wind velocity in the low-resolution domain, and N_{n_p} is the number of points in a polar grid on wake plane n_p of the given wind turbine. The polar grid on a given wake plane has a uniform radial and azimuthal discretization equal to the average spatial

[¶]For example, TurbSim¹⁹ or Mann model inflow can be used, which is propagated through the wind farm using Taylor's frozen turbulence assumption. Such inflow is most applicable to small wind farms or a subset of a wind turbines within a larger wind farm.

[#]This atmospheric precursor simulation captures more physics than synthetic turbulence—including atmospheric stability, wind farm-wide turbulent length scales, and complex terrain effects. It is more computationally expensive than using the simple ambient wind modeling options, but it is orders of magnitude less computationally expensive than a SOWFA simulation with wind turbines present.

discretization of the low-resolution domain— independent from the radial finite-difference grid used within the wake dynamics module— and a diameter of $C_{Meander} D_{np}^{Wake}$, $C_{Meander}$ is discussed below. Subscript n is appended to \vec{V}_{Amb} in Equation (8) to identify wind data that have been trilinearly interpolated from the 3D low-resolution domain to the polar grid on the wake plane.

The ambient wind submodel also calculates as output the ambient TI around each rotor, TI_{Amb} , using Equation (9).

$$TI_{Amb} = \sqrt{\frac{\frac{1}{3N_{np}} \sum_{n=1}^{N_{np}} \left\| \vec{V}_{Amb,n} - \frac{1}{N_{np}} \sum_{n=1}^{N_{np}} \vec{V}_{Amb,n} \right\|_2}{\left\| \frac{1}{N_{np}} \sum_{n=1}^{N_{np}} \vec{V}_{Amb,n} \right\|_2}} \Big|_{n_p=0} \quad (9)$$

In contrast to the common definition of TI used in the wind industry, which consists of a time-averaged quantity of the axial wind component, the TI calculated in the ambient wind submodel is based on a uniform spatial average of the three vector components. Not using time averaging ensures that only ambient wind at the current time step needs to be processed, which increases computational efficiency. Moreover, any time variation in the spatial average is moderated by the low-pass time filter in the wake dynamics module. Using spatial averaging and the three vector components allows for atmospheric shear, wind veer, and other ambient wind characteristics to influence the eddy viscosity and wake deficit evolution in the wake dynamics module. The incorporation of wake-added turbulence is left for future work. Note that Equation (9) uses the eight wind data points from the low-resolution domain surrounding each point in the polar grid rather than interpolation. This is because calculating wind data in the polar grid on the wake plane via trilinear interpolation from the low-resolution domain would smooth out spatial variations and artificially reduce the calculated TI.

Wake merging

In previous implementations of DWM, the wind turbine and wake dynamics were solved individually or serially, not considering two-way wake-merging interactions. Additionally, there was no method available to calculate the disturbed wind in zones of wake overlap. In FAST.Farm, the wake-merging submodel identifies zones of wake overlap between all wakes across the wind farm by finding wake volumes that overlap in space. Wake deficits are superimposed in the axial direction based on the root sum squared (RSS) method;²² transverse components (radial wake deficits) are superimposed by vector sum. In Katicc et al.,²² the RSS method is applied to wakes with axial deficits that are uniform across the wake diameter, and radial deficits are not considered. In contrast, the RSS method in FAST.Farm is applied locally at a given wind data point. The RSS method assumes that the local kinetic energy of the axial deficit in a merged wake equals the sum of the local energies of the axial deficits for each wake at the given wind data point.

The disturbed wind velocities across the low-resolution domain, \vec{V}_{Dist} , are computed using Equation (10).

$$\vec{V}_{Dist} = \vec{V}_{Amb} - \bar{\vec{x}} \sqrt{\sum_{n=1}^{N^{Wake}} \left\{ (\bar{\vec{x}})^T \left(V_{x_n}^{Wake} \hat{x}_n + V_{r_n}^{Wake} \hat{r}_n \right) \right\}^2} + \sum_{n=1}^{N^{Wake}} \left[\left\{ I - \bar{\vec{x}} (\bar{\vec{x}})^T \right\} \left\{ V_{x_n}^{Wake} \hat{x}_n + V_{r_n}^{Wake} \hat{r}_n \right\} \right] \quad (10)$$

Here, \hat{x}_n is the axial orientation; \hat{r}_n is the radial unit vector; N^{Wake} is the number of wake volumes overlapping a given wind data point in the wind domain; $\bar{\vec{x}}$ is the weighted-average axial orientation associated with a given point in the wind spatial domain; $\{\bar{\vec{x}}\}^T$ projects $\{V_{x_n}^{Wake} \hat{x}_n + V_{r_n}^{Wake} \hat{r}_n\}$ along $\bar{\vec{x}}$; and $[I - \bar{\vec{x}} (\bar{\vec{x}})^T]$ calculates the transverse component of $\{V_{x_n}^{Wake} \hat{x}_n + V_{r_n}^{Wake} \hat{r}_n\}$ normal to $\bar{\vec{x}}$.

Subscript n is used to identify each wake volume overlapping a given wind data point in the wind domain. The first, second, and third terms on the right-hand side of Equation (10) represent the ambient wind velocity, the RSS superposition of the axial wake velocity deficits, and the vector sum of the transverse wake velocity deficits, respectively. Wake volume n_p starts at wake plane n_p and extends to wake plane $n_p + 1$. The vector quantity $\{V_{x_n}^{Wake} \hat{x}_n + V_{r_n}^{Wake} \hat{r}_n\}$ represents the total wake velocity deficit associated with where the given wind data point lies within the specific wake volume and corresponding wake plane. Because each wake plane may have a unique orientation, what constitutes “axial” and “radial” in the superposition at a given wind data point is determined by weighted averaging the orientations of each wake volume overlapping that point (weighted by the magnitude of each axial wake deficit). A similar equation (not shown) is used to calculate the disturbed wind velocities across the high-resolution domain for each turbine, which is needed to calculate the disturbed wind inflow to a turbine. Note that for the high-resolution domain, a turbine is prevented from interacting with its own wake.

Once the distributed wind velocities across the low-resolution domain have been found, the wake-merging submodel computes the advection, deflection, and meandering velocity of each wake plane, \vec{V}_{n_p} , for each turbine as the weighted spatial average of the disturbed wind velocity across the wake plane, using Equation (11).

$$\vec{V}_{n_p} = \frac{\sum_{n=1}^{N_{np}} w_n \vec{V}_{Dist_n}}{\sum_{n=1}^{N_{np}} w_n} \quad (11)$$

Unlike Equation (8), Equation (11) includes a spatial weighting factor, w_n , dependent on the radial distance of point n from the center of the wake plane described below. FAST.Farm specifies the meandering velocity of each wake plane to zero for any wake plane that has entirely left the boundaries of the low-resolution domain. Larsen et al.¹¹ proposed a uniform spatial average where all points within a circle of diameter $2D_{n_p}^{Wake}$ are given equal weight. However, the Fourier transform of the circular function in a polar spatial domain results in a *jinc* function in the polar wave number domain, implying a gentle roll off of energy below the cut-off wave number and pockets of energy at distinct wave numbers above the cut-off wave number. Experience with FAST.Farm development has shown that this approach results in less overall wake meandering and at improper frequencies. As such, three weighted spatial averaging methods have been implemented in FAST.Farm, as defined in Equation (12).

$$w_n = \begin{cases} 1 \\ jinc\left(\frac{r_n}{C_{Meander}D^{Wake}}\right) \\ jinc\left(\frac{r_n}{C_{Meander}D^{Wake}}\right)jinc\left(\frac{r_n}{2C_{Meander}D^{Wake}}\right) \end{cases} \quad (12)$$

The first method is a spatial average with a uniform weighting with a local polar grid diameter of $C_{Meander}D^{Wake}$ at wake plane n_p , resulting in a cut-off wave number of $\frac{1}{C_{Meander}D^{Wake}}$. The second and third methods weight each point in the spatial average by a form of the *jinc* function dependent on radius of the point from the wake centerline, r_n , normalized by $C_{Meander}D^{Wake}$. This results in a more ideal low-pass filter with a sharper cut-off of energy in the polar wave number domain with a cut-off wave number of $\frac{1}{C_{Meander}D^{Wake}}$. However, because the *jinc* function decays slowly with increasing argument, the *jinc* function must be windowed to be applied in practice. The second method truncates the *jinc* function at its first zero crossing. The third method windows the *jinc* function by multiplying it with a *jinc* function of half the argument, which tapers the weighting to zero at its second zero crossing. These weighted spatial averaging methods improve the overall level and frequency content of the wake meandering at the expense of a bit heavier computations due to the larger polar grid diameters.[¶] A value of $C_{Meander} = 2$ follows from the characteristic dimension important to transverse wake meandering proposed by Larsen et al.¹¹ The user-specified calibration parameter $C_{Meander}$ is included in all methods to enable the user of FAST.Farm to better match the meandering to known solutions. Note that the lower the value of $C_{Meander}$, the more the wake will meander.

2.2 | Modeling cases and setup

Several modeling cases involving different 2000-s precursor wind inflow data were used to compare turbine performance and structural response between LES and FAST.Farm simulations. All cases used 8 m/s mean hub height wind speed with variations in TI and shear exponents, as summarized in Table 1. The selected cases represent key situations where the use of FAST.Farm would be applicable. This work focuses on a single below-rated wind speed with high and low TI and shear, which are representative of cases where wake effects are most important for wind farm power performance. The case with yaw error exemplifies a situation where the wakes from upstream turbines are purposely steered away from the downstream turbines, although some wake-turbine interaction still occurs. For this simulation, turbine yaw angles were held constant for the entire simulation. Further details of each inflow case are provided in Jonkman et al.⁵ Each precursor was generated in SOWFA without turbines present. The precursors were then used as input to LES and FAST.Farm simulations of a small wind farm with three laterally aligned NREL 5-MW reference wind turbines separated by $8D$. For all simulations, tower influence on the flow and nacelle blockage are not considered. All model coefficients in FAST.Farm were set to the default values.¹³ An instantaneous wake visualization of Case V8_TI10 simulated in FAST.Farm is shown in Figure 3.

TABLE 1 Case description for turbine structural response comparison

Case name	Hub height wind speed	Turbulence intensity	Shear exponent	Yaw error
V8_TI10	8 m/s	10%	0.2	0°
V8_TI10_yaw	8 m/s	10%	0.2	10°/10°/0°
V8_TI6	8 m/s	6%	0.1	0°

[¶]The truncated *jinc* method has roughly 50% more points within the polar grid than the uniform method, and the windowed *jinc* method has roughly five times as many points than the uniform method.

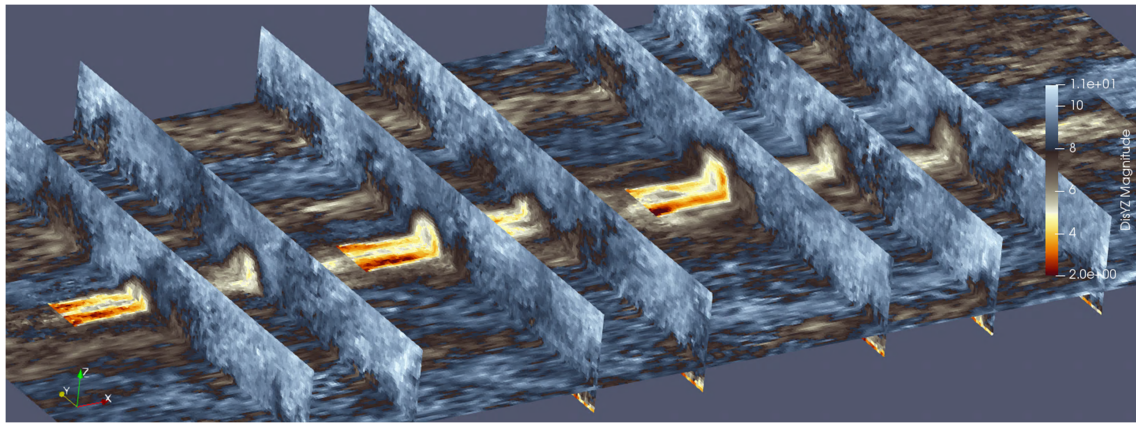
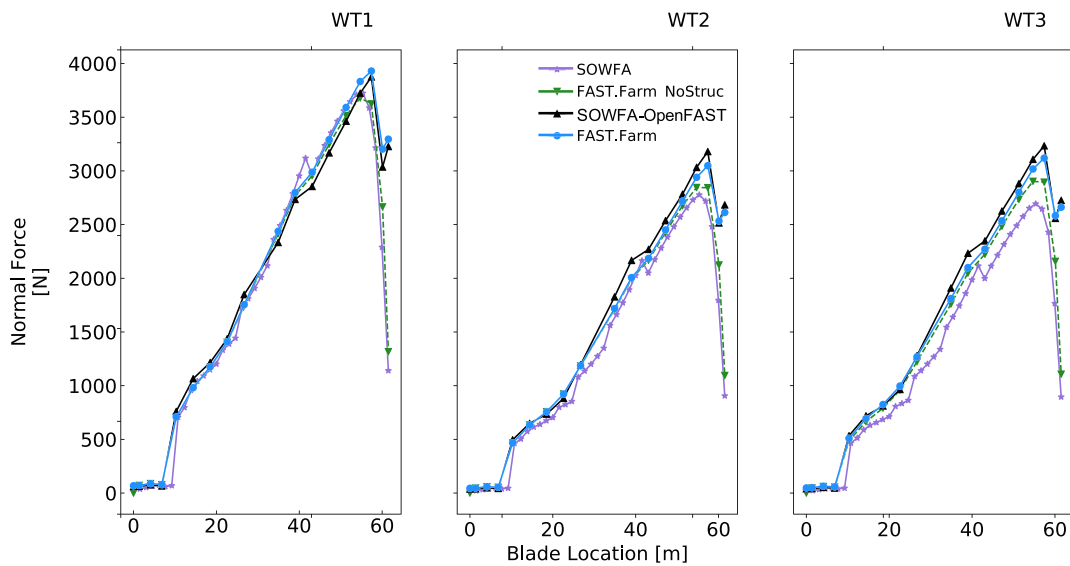


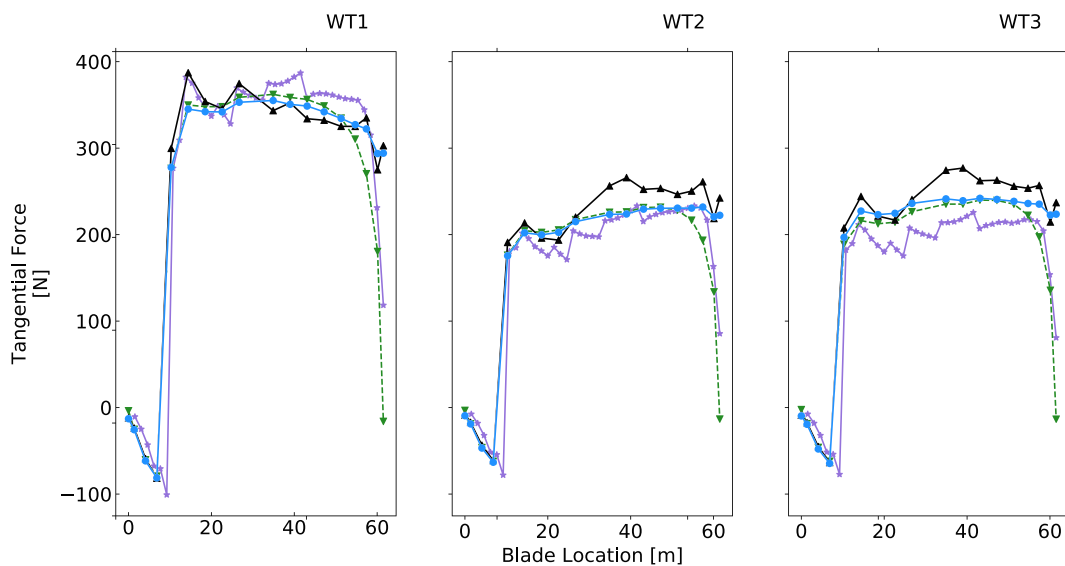
FIGURE 3 Instantaneous 2D flow visualization of a three-turbine FAST.Farm simulation with 8 m/s high-turbulence inflow (Case V8_TI10), colored by velocity magnitude. The horizontal slice is sampled at hub height and vertical slices are sampled at 3D and 5D downstream of each turbine [Colour figure can be viewed at wileyonlinelibrary.com]

Turbine performance is compared for both rigid and flexible turbine simulations. When SOWFA is not coupled to OpenFAST, the turbines are modeled rigidly, with only the rigid body rotation of the rotor considered as a single structural degree of freedom (DOF). The FAST.Farm equivalent of this is disabling all structural DOFs in OpenFAST except the generator DOF (FAST.Farm_NoStruc). In SOWFA-OpenFAST, OpenFAST is coupled to LES using an actuator line model to enable turbine structural response calculations within LES using the OpenFAST structural model ElastoDyn.³ When SOWFA is coupled to OpenFAST, current modeling limitations do not allow for tip- or hub-loss corrections available in OpenFAST to be used. Because the aerodynamic load distribution in the SOWFA-OpenFAST results is calculated from the OpenFAST side, this leads to differences between SOWFA and SOWFA-OpenFAST blade load results. Though it is considered best practice to include such corrections for the conditions simulated in this work, flexible FAST.Farm simulations were also run without these corrections to allow for more comparable modeling conditions. However, tip- and hub-loss corrections are included for the rigid turbine simulations. Therefore, it is expected that turbine performance will differ slightly between the rigid and flexible simulation results and more so than they would solely from considering deflection or not. The differences in blade span forces resulting from these modeling choices are shown in Figure 4. Here, time-averaged normal and tangential forces along the blade span are shown for Case V8_TI10_Yaw. Note that the FAST.Farm blade discretization is coarser than the SOWFA blade discretization. When comparing FAST.Farm and SOWFA-OpenFAST results, this will result in differences in the respective load distributions. However, this is expected to be a negligible source of discrepancy, given that each solution uses a discretization that is numerically converged. There are minimal differences in normal and tangential forces between all methods along the majority of the blade span until $\sim 0.86R$, at which point the structurally rigid results sharply drop, as expected when a tip-loss correction is used. However, the structurally flexible turbine results remain higher due to a tip-loss correction not being used in these models. As mentioned above, SOWFA-OpenFAST modeling limitations do not allow for tip- or hub-loss corrections to be applied, and the structurally flexible FAST.Farm simulations were also run without such corrections for consistency. The differing blade tip force load will result in differing turbine response, most notably higher power, torque, and rotor speed corresponding to a higher blade tip force load. The small bump in the SOWFA normal force at $r = 40$ m is due to changes in airfoil shapes at those locations. This uptick is not seen in FAST.Farm results because there is no output blade node located at that position. Similarly, the jumps in the SOWFA tangential force along the blade span correspond to changes in airfoil shapes at those locations. A summary of the simulation approach details is provided in Table 2.

Turbine performance in terms of generator power, generator torque, and rotor speed are discussed briefly because structurally flexible turbine comparisons have not previously been made between SOWFA-OpenFAST and FAST.Farm. Turbine structural response is the focus of this study. Specifically, turbine structural response was quantitatively studied by comparing time series, power spectra, and statistical results of out-of-plane (OoP) and in-plane (IP) bending and pitching blade root moments; low-speed shaft bending in the rotating frame; fore/aft (FA) and side/side (SS) bending and yaw moments at the tower-top and tower-base; and OoP blade tip displacements, as detailed in Table 3. Such comparisons will allow for structural response similarities and differences between the models to be quantified and help to inform sources of discrepancy in future planned validation studies and model improvements. To aid in determining the importance of wake-added turbulence, the wake response is analyzed for Case V8_TI6 by comparing the time-averaged TI, mean, and standard deviation of the hub height u -component of velocity for varying downstream distances. These wake-based quantities are not available for Case V8_TI10. However, further analysis of wake behavior for these cases is included in Jonkman et al.⁵ This work has shown better agreement in wake meandering between SOWFA and FAST.Farm results for simulations with highly turbulent ambient inflow, indicating that wake-added turbulence is not as important for such cases.



(A) Time-averaged blade span normal force.



(B) Time-averaged blade span tangential force.

FIGURE 4 Time-averaged blade span (a) normal and (b) tangential force from all methods for the case with 8 m/s highly turbulent inflow, with the first two turbines yawed to 10° (Case V8_TI10_Yaw) [Colour figure can be viewed at wileyonlinelibrary.com]

TABLE 2 Simulation approach details

Simulation approach	Structural method	Tip/hub corrections
SOWFA	Rigid body	Enabled
SOWFA-OpenFAST	ElastoDyn	Disabled
FAST.Farm_NoStruct	Rigid body	Enabled
FAST.Farm	ElastoDyn	Disabled

In addition to relative accuracy, it is important to consider computational time of each simulation. All simulations were run on dual Intel Xeon Gold 6154 processors. SOWFA and SOWFA-OpenFAST simulations were run on 1000 processors for ~14.5 and ~16.5 wall time hours, respectively. FAST.Farm simulations were run on 36 processors for 1.3 wall time hours. These values do not include the time required to generate the

TABLE 3 Structural quantities of interest (QoI)

Quantity of interest	Component		
Blade root moments	OoP bending	IP bending	Pitching moment
Low-speed shaft moment at main bearing	0° bending	90° bending	
Tower-top moments	FA bending	SS bending	Yaw moment
Tower-base moment	FA bending	SS bending	Yaw moment
Blade tip displacements	OoP	IP	
Tower-top deflections	FA	SS	

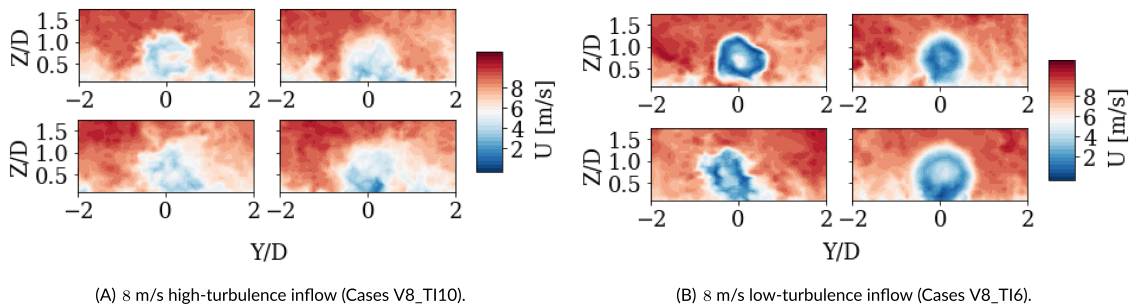


FIGURE 5 Instantaneous 2D flow visualization of a three-turbine SOWFA and FAST.Farm simulation with 8 m/s inflow, Cases (a) V8_TI10 and (b) V8_TI6, colored by velocity magnitude. For each case, the vertical slices are sampled at 2D downstream of WT1 (top) and WT2 (bottom) for SOWFA (left) and FAST.Farm (right) results [Colour figure can be viewed at wileyonlinelibrary.com]

inflow wind conditions. This corresponds to roughly 300× more computational time required for SOWFA and SOWFA-OpenFAST simulations than FAST.Farm simulations.**

3 | RESULTS

This section describes the results from SOWFA, SOWFA-OpenFAST, and FAST.Farm for the cases listed in Table 1 with both structurally rigid (FAST.Farm_NoStruc) and flexible (FAST.Farm) turbine modeling. Wake response differences for SOWFA and FAST.Farm turbine modeling are assessed by comparing instantaneous flow visualizations and average TI values in the wakes. Turbine operation differences from all methods are quantitatively assessed by comparing average normal force along the blade span and time series and statistical results of generator power, generator torque, and rotor speed. The remainder of the paper is focused on differences in structural responses from SOWFA-OpenFAST and FAST.Farm with structurally flexible turbine modeling. These differences are assessed by comparing time series, statistical results, and power spectral densities (PSDs) of the QoIs listed in Table 3. Additionally, percent differences between the results are compared across the QoIs and turbines to identify components or situations that lead to especially comparable or differing results.

3.1 | Wake response

Instantaneous flow visualizations of three-turbine SOWFA and FAST.Farm simulations are shown in Figure 5 for Cases V8_TI10 and Cases V8_TI6. Vertical slices are sampled 2D downstream of WT1 (top) and WT2 (bottom) for SOWFA (left) and FAST.Farm (right) results. For both cases, the ambient inflow outside the wake flow compares well for SOWFA and FAST.Farm results, indicated by similar large-scale structures. This is expected since the same inflow is used in each simulation. For Case V8_TI10, comparable wake structures are seen between SOWFA and FAST.Farm results for both WT1 and WT2, especially in terms of wake breakdown. This is qualitatively shown by the noncircular nature of the wakes. For high TI inflows, the ambient TI is sufficient to distort the background wake structure. This leads to FAST.Farm predicting wakes that qualitatively resemble the wakes from SOWFA results. However, the extent of wake breakdown differs between FAST.Farm and SOWFA results for Case V8_TI6. Here, the wake deficits behind WT1 are fairly similar, but the SOWFA results show that the wake structure begins to break

**The number of processors was not optimized here. When running parallel FAST.Farm simulations with T turbines and N processors, $N - (T + 1)$ processors remain idle when OpenFAST is advancing in time because one processor is used for each OpenFAST model (totaling T processors), while one processor is used to process ambient wind data for the next FAST.Farm time step. All N processors are used only in the ambient wind and array effects module. Further computational gain between FAST.Farm and LES is possible by optimizing code parallelization.

down. The wake structures behind WT2 are quite different, with the SOWFA results showing significant wake breakdown, while the FAST.Farm results show a fairly circular wake. For low TI inflows, the ambient TI is not sufficient to distort the wake structure in FAST.Farm, whereas in SOWFA, the strong wake shear layer is driving wake breakdown. Moreover, the wake breakdown in SOWFA will induce additional wake meandering not captured by FAST.Farm. These differences in wake breakdown and meandering will lead to differing power outputs and structural responses when comparing FAST.Farm and SOWFA results. Such discrepancies highlight the importance of wake-added turbulence, which is not currently modeled in FAST.Farm.

Time-averaged hub height TI, mean u-velocity, and standard deviation of u-velocity values computed for varying downstream distances are shown in Figure 6 for SOWFA and FAST.Farm results from Case V8_TI6. These results show a stark difference between SOWFA and FAST.Farm results for TI levels in the turbine wakes. Directly upstream of the first turbine, all inflow quantities are nearly identical due to the use of the same inflow. However, FAST.Farm predicts an average wake TI of 8.8%, or an increase of 1.6 \times above freestream TI, for all downstream distances, whereas SOWFA predicts an average wake TI of 14.1%, or an increase of 2.6 \times above freestream TI. That is, the increase in TI driven by the wake is much higher in SOWFA simulations. Additionally, FAST.Farm-predicted wake TI values vary by 1.9% across all downstream distance, whereas SOWFA predicts a variation of 8.5% across the same distances. Mean u-velocity results are comparable for all distances, with an average percent difference of 10.9% and the error concentrated in the near-wake behind each turbine, where FAST.Farm is not expected to predict accurate wake behavior because the near-wake correction model is only intended to provide accurate far-wake response. Therefore, the discrepancies in wake TI are due largely to differences in standard deviation of the u-velocity in the wake of the turbines. This quantity is shown to follow comparable trends to those of the TI results, with SOWFA results increasing above ambient levels by up to 201%. Alternatively, FAST.Farm standard deviation results only increase up to 124% and reduce below ambient level by up to 9.2%. These drastic differences are due to the consideration of wake breakdown and breakdown-driven wake meandering in SOWFA, which is not captured by FAST.Farm. Such quantities will directly impact downstream turbine power production and structural loading. This reinforces the importance of including a wake-added turbulence model in FAST.Farm in the future to accurately predict wake behavior and turbine response in simulations with low ambient TI.

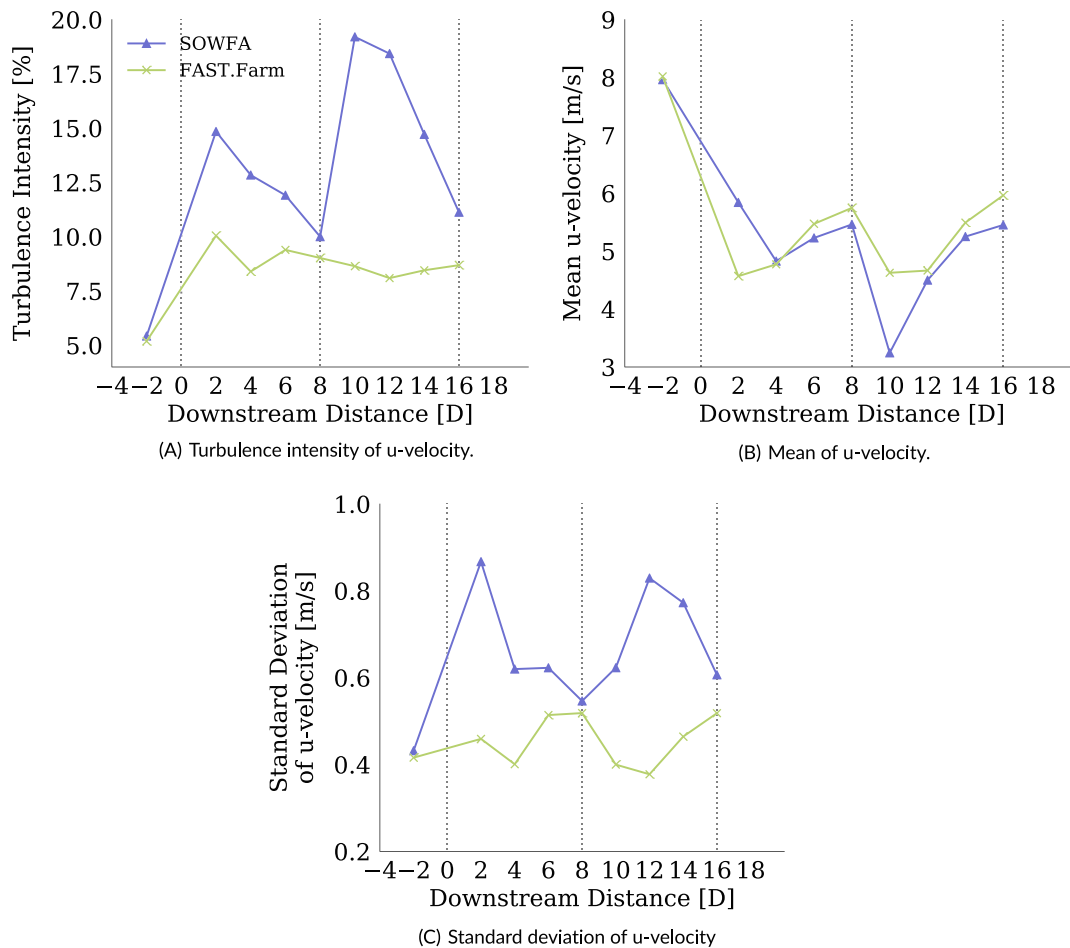


FIGURE 6 Time-averaged hub height turbulence intensity values at varying downstream distances for SOWFA and FAST.Farm results with 8 m/s low-turbulence inflow (Case V8_TI6). Dashed vertical lines indicate downstream turbine locations [Colour figure can be viewed at wileyonlinelibrary.com]

3.2 | Turbine performance response

Time series and probability density function (PDF) results of the turbine generator power, generator torque, and rotor speed for Case V8_T110 are shown in Figures 7 and 8, respectively. For all quantities, the time series from all models are quite consistent with each other for the upstream turbine (WT1). This is expected because the same ambient inflow is used for all simulations. Note that the structurally rigid simulation results are not expected to agree with the flexible simulation results. In particular, the trends in terms of higher generator power and torque mirror the trends seen in blade tip normal force. Larger differences are seen in the downstream turbine time series, largely due to differences in wake behavior. Previous studies⁵ have shown that the FAST.Farm wake meandering time series for the first turbine closely matches that from SOWFA for ambient wind inflow with high TI. However, time series results do not compare as well for more downstream turbines. Additionally, the wake breakdown-

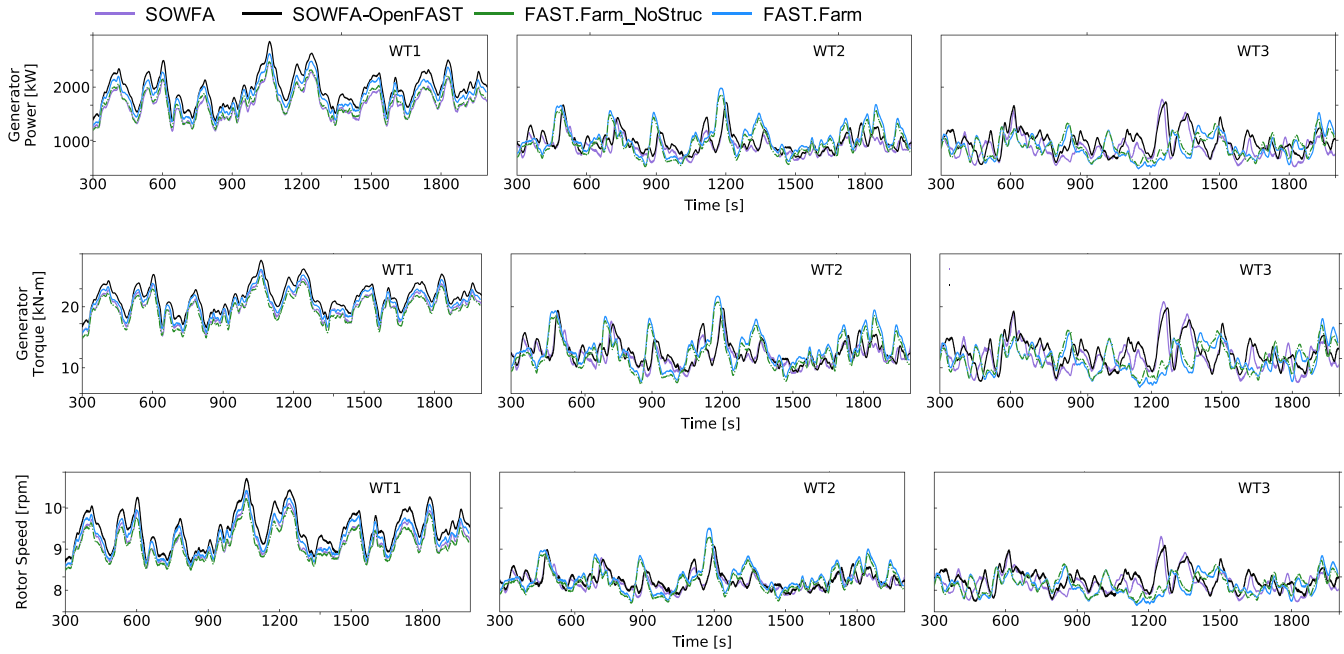


FIGURE 7 Time series of generator power, generator torque, and rotor speed for all turbines for the case with 8 m/s high-turbulence inflow (Case V8_T110) [Colour figure can be viewed at wileyonlinelibrary.com]

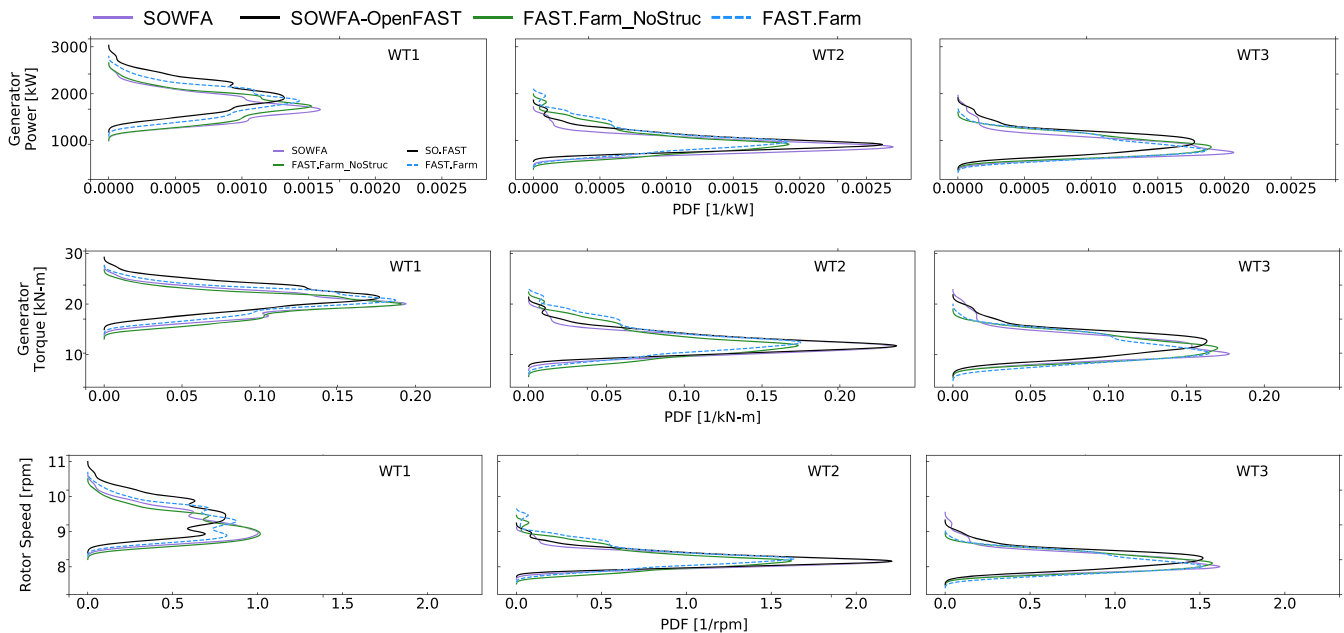


FIGURE 8 Probability density function of generator power, generator torque, and rotor speed for all turbines for the case with 8 m/s high-turbulence inflow (Case V8_T110) [Colour figure can be viewed at wileyonlinelibrary.com]

induced added turbulence—not presently considered in FAST.Farm—influences the wake dynamics more for ambient inflow with lower TI and for downstream turbines. Wake effects result in loss of power for the downstream turbine, which is captured by all methods. PDFs are shown for the same quantities in Figure 8. Here, PDFs are computed using 20 bins to show asymmetries in the results. Statistically, close agreement is seen between the SOWFA and rigid FAST.Farm simulations, in particular for generator torque and rotor speed and between SOWFA-OpenFAST and flexible FAST.Farm results. In particular, asymmetries are captured well for each quantity and across all turbines. PDF results of generator power for all cases are shown in Figure 9. Similar comparisons are seen for WT1 across all cases, particularly for rigid turbine response. Flexible turbine results also compare well, but stronger differences are seen. Larger differences are seen for the flexible turbine results because of the increased complexity of the problem due to aeroelastic effects. However, asymmetries of downstream turbine results are not captured as well for cases V8_T110_Yaw and V8_T16. The differences seen in Case V8_T110_Yaw is likely due to the absence of a curled wake model in FAST.Farm. The differences seen in Case V8_T16 are likely due to the importance of wake-added turbulence, as discussed in Section 3.1, which is not currently captured in FAST.Farm.

Quantitative differences between turbine response results are found using the percent difference between cases, as defined in Equation (13).

$$\%D(\bar{x}) = \left| \frac{\bar{X}_{FAST.Farm} - \bar{X}_{SOWFA}}{\left(\frac{x + \bar{X}_{SOWFA}}{2}\right)} \right| \times 100 \tag{13}$$

These percent difference values were computed for average mean and standard deviation values between SOWFA and structurally rigid FAST.Farm results, as well as SOWFA-OpenFAST and structurally flexible FAST.Farm results for each turbine response component and case. These results are summarized in Figure 10, with percent difference of mean values (%D(\bar{x})) shown in Figure 10a,c, and percent difference of standard deviation values (%D(σ)) shown in Figure 10b,d. Structurally rigid turbine results are shown in the top row and flexible turbine results in the bottom row. Note the difference in y-axis scale between each plot. Overall, average %D(\bar{x}) results remain below 5%, and average %D(σ) results remain below 25% for both structurally rigid and flexible turbine results, indicating that more differences between results arise due to transient response rather than mean quantities or structural properties.

3.3 | Structural response

The structural response of FAST.Farm with structurally flexible wind turbines is assessed by comparing time series, statistical results, and PSDs for blade root OoP bending moments against SOWFA-OpenFAST. Additionally, the tower-base FA bending moments are investigated using

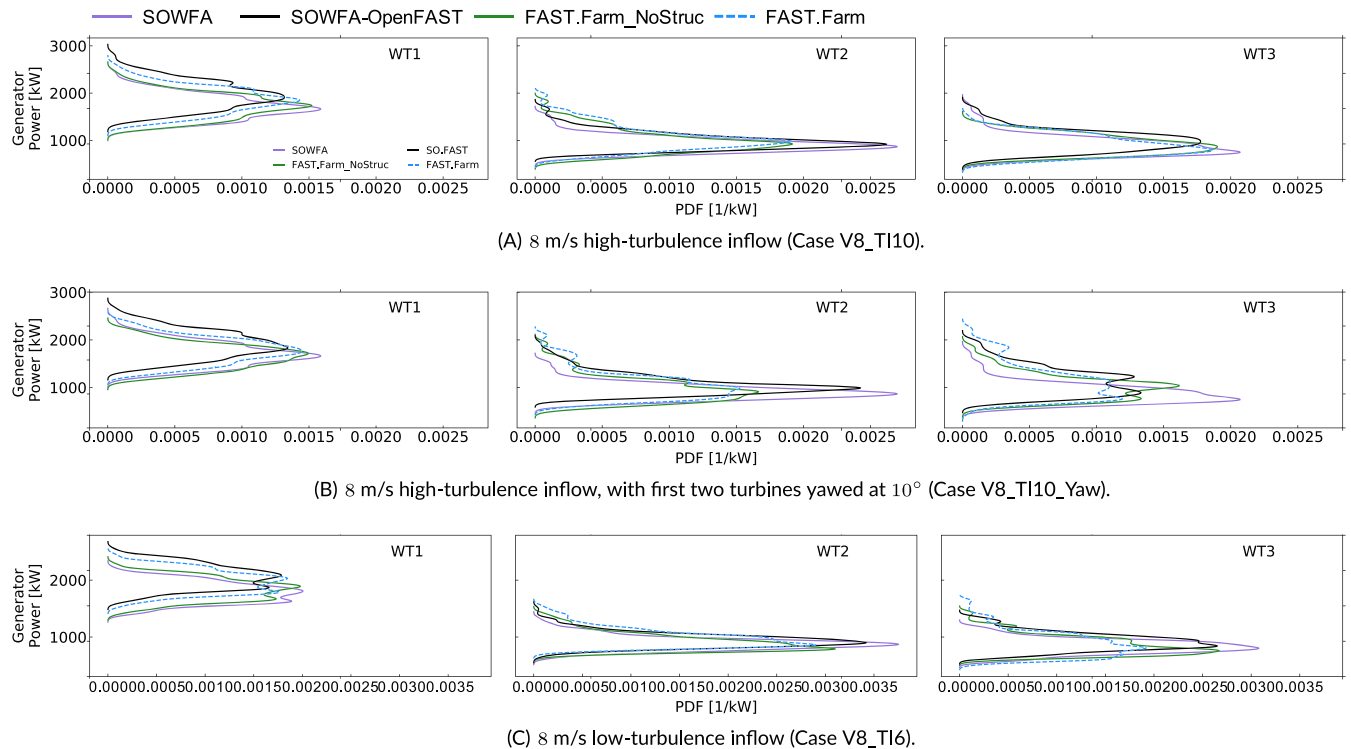
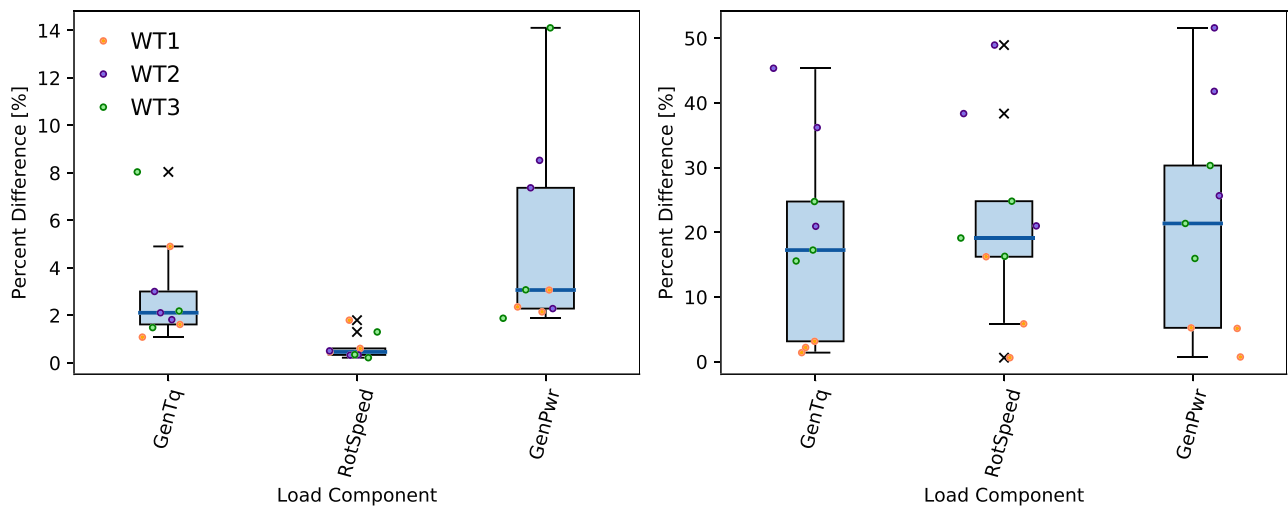
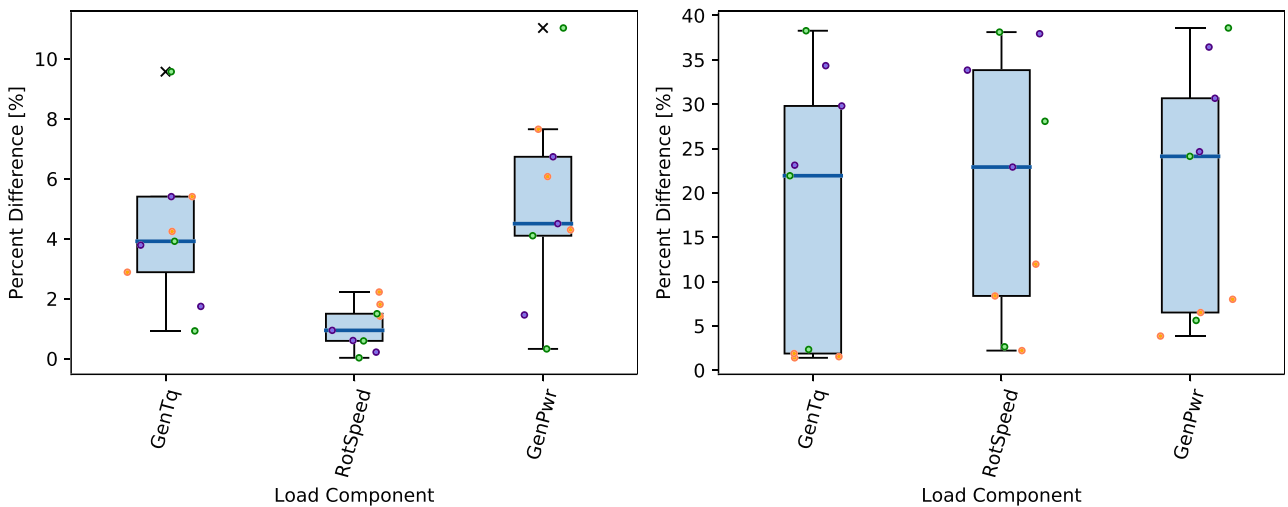


FIGURE 9 Probability density function of generator power for all turbines in all cases [Colour figure can be viewed at wileyonlinelibrary.com]



(A) Percent difference of mean values between SOWFA and rigid FAST.Farm results. (B) Percent difference of standard deviation values between SOWFA and rigid FAST.Farm results.



(C) Percent difference of mean values between SOWFA-OpenFAST and flexible FAST.Farm results. (D) Percent difference of standard deviation values between SOWFA-OpenFAST and flexible FAST.Farm results.

FIGURE 10 Box and whisker plots of percent difference by turbine performance component. Each dot represents an individual case and turbine result (variation in x-axis location within a bar aids visualization). Dots are colored by turbine number. Box and whisker plots show the median (blue line) value of all results; lower and upper quartile values (black lines); maximum and minimum values excluding outliers (whiskers); and outlier points (x symbols) [Colour figure can be viewed at wileyonlinelibrary.com]

statistical and PSD results to show a comparison of results further down the load path. Finally, percent differences between the results are compared for all QoIs listed in Table 3 to identify components or situations that lead to especially comparable or differing results.

3.3.1 | Detailed results

The next three figures (Figures 11 to 13) show time series, probability distributions, and power spectra for blade root OoP bending moment for the three simulated wind turbines. Time series and PDF results of the turbine blade root OoP bending moment for Case V8_TI10 are shown in Figure 11. As with turbine response results, strong agreement is seen between time series results for WT1, with increased differences for downstream turbines. PDF results also show strong agreement for all turbines. PDF results of blade root OoP bending for all cases are shown in Figure 12. Strong agreement is seen for all WT1 results, though SOWFA-OpenFAST produces a higher mean blade root OoP bending moment for all simulation cases. Model agreement for downstream turbines reduces for the cases with yaw error and low TI.

PSD results of blade root OoP bending moment are shown in Figure 13 for each simulation case. The spike in the PSDs at zero frequency corresponds to the time series mean value, which is similar for all cases and turbines. The subsequent peaks correspond to the nP passing

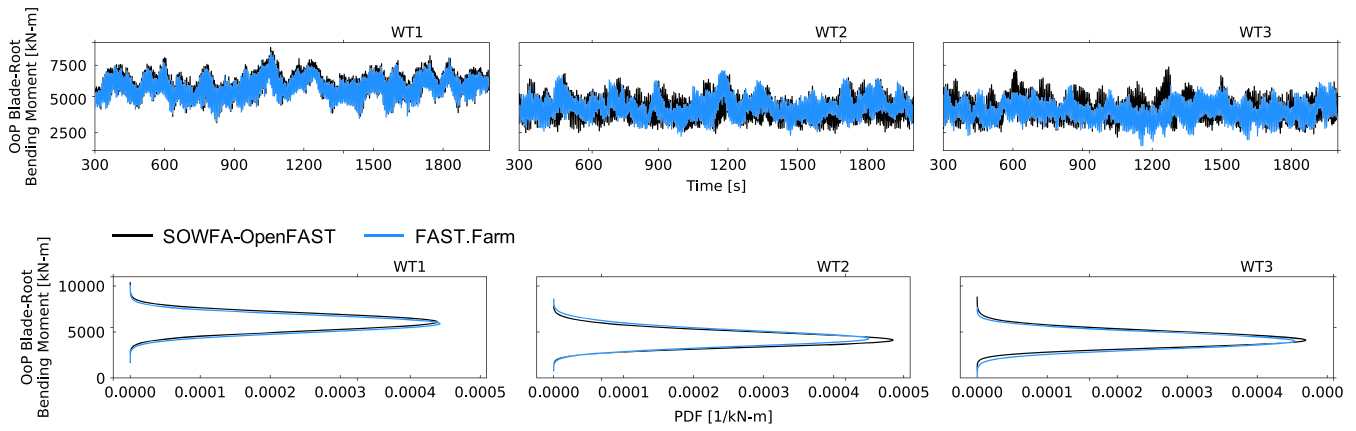
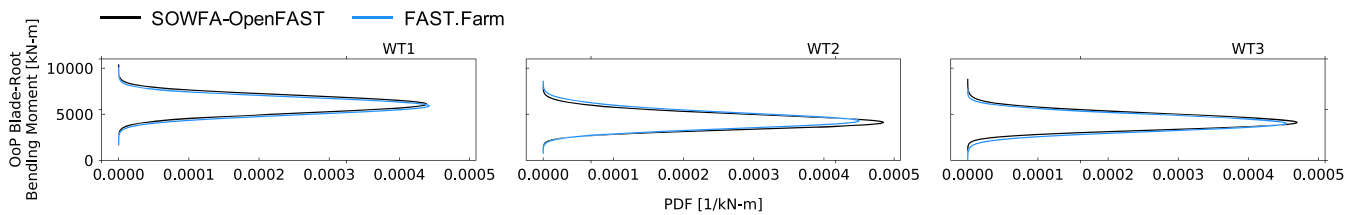
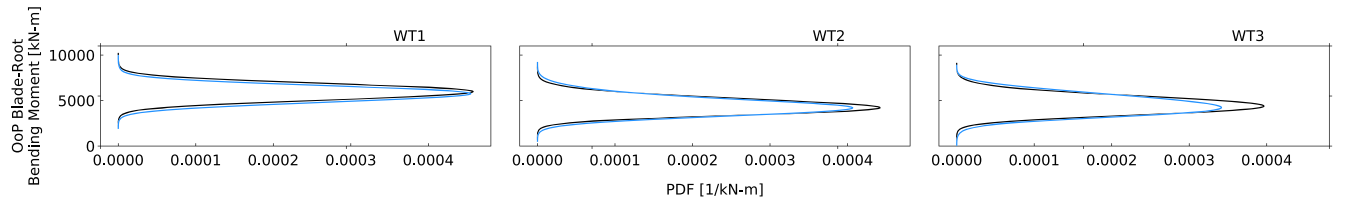


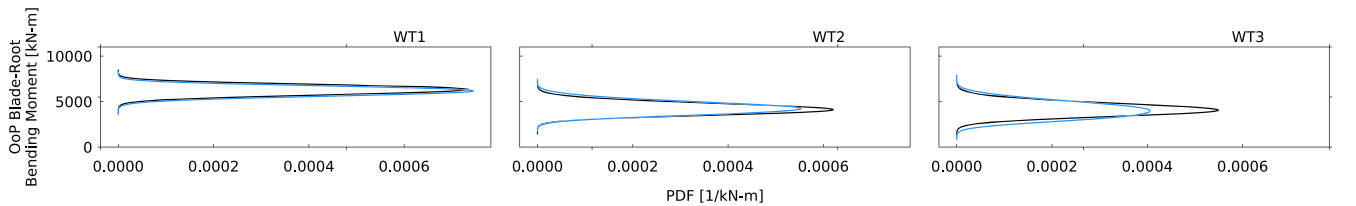
FIGURE 11 Time series and probability density function of blade root OoP bending moment for the case with 8 m/s high-turbulence inflow (Case V8_TI10) [Colour figure can be viewed at wileyonlinelibrary.com]



(A) 8 m/s high-turbulence inflow (Case V8_TI10).



(B) 8 m/s high-turbulence inflow, with first two turbines yawed at 10° (Case V8_TI10_Yaw).



(C) 8 m/s low-turbulence inflow (Case V8_TI6).

FIGURE 12 Probability density function of blade root OoP bending moment results for all cases [Colour figure can be viewed at wileyonlinelibrary.com]

frequencies.^{††} There is close agreement for WT1 1P magnitude for Cases V8_TI10 and V8_TI6; reduced agreement is seen for Case V8_TI10_Yaw due to the introduction of turbine yaw, which suggests some difference between the LES-generated induction field and that produced by the skewed wake model of blade element/momentum in OpenFAST. Note that the 1P peaks for the V8_TI10_Yaw case are larger than for the V8_TI10 case, but not as much as would be expected given the skewed flow in the former case. The sizeable 1P peaks in both cases are likely the result of the sizeable shear exponent used for both cases. For WT2 and WT3, there is good agreement of the 1P magnitude for cases V8_TI10 and V8_TI10_Yaw, with reduced agreement for Case V8_TI6, especially for WT3, where FAST.Farm predicts higher 1P excitation than SOWFA-OpenFAST. This suggests that the wake of FAST.Farm is more affected by the atmospheric boundary layer shear layer than that of SOWFA-OpenFAST, whose increased wake distortion from a Gaussian distribution and wake-added turbulence diminishes the wake shear layer. The 2P

^{††}Passing frequencies are defined as $n\bar{\Omega}$, where n is an integer and $\bar{\Omega}$ is the average turbine rotor speed expressed in hertz.

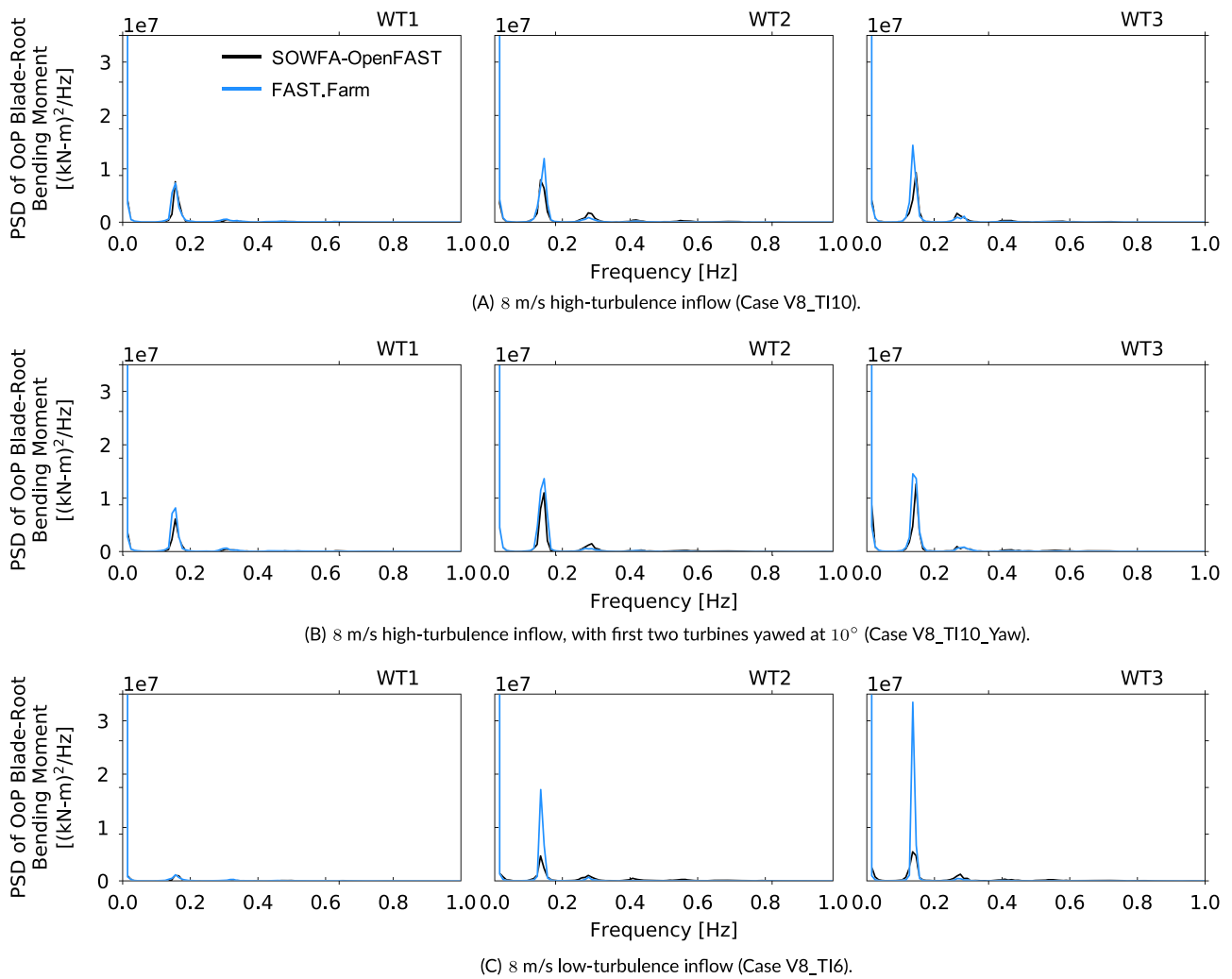


FIGURE 13 Power spectral density of blade root OoP bending moment results for all cases [Colour figure can be viewed at wileyonlinelibrary.com]

magnitude—though less energetic than $1P$ —is increased in the downstream turbines relative to WT1 for all cases, with SOWFA-OpenFAST predicting a higher $2P$ excitation than FAST.Farm. This suggests more high-frequency energy content in the LES-generated wake than in FAST.Farm. Note that though only blade root OoP bending moments are shown here, comparable similarities and differences are seen for the remaining blade QoIs.

While overall good agreement is seen for turbine blade QoIs, turbine load QoIs further down the load path produced less comparable results between solutions. PDF and PSD results for tower-base FA bending moments from Case V8_TI10 are shown in Figure 14. The statistical distribution of load values was overall similar between the simulation approaches. The spectral analysis, however, shows that the solutions do differ at certain blade-passing frequencies. In particular, the wake is exciting the $3P$ frequency more in SOWFA-OpenFAST than in FAST.Farm. The $3P$ excitation in the fixed frame is caused by the nP excitation for the lowest modes (small n) in the rotating frame of the rotor. The higher $3P$ excitation in SOWFA-OpenFAST versus FAST.Farm suggests more high-frequency energy content in the LES wake than in the wake of FAST.Farm. Similar differences in PSD results are seen for tower-base and tower-top yaw torsion moment, tower-top FA moment, and FA tower-top deflection (not shown).

3.3.2 | All components and cases

As was done for turbine performance results, quantitative differences between structural response results are shown using the percent difference across turbines and cases. These results are summarized in Figure 15a,b, separated by load QoI. Note that mean low-speed shaft bending moments; tower-top FA bending moment; and tower-top and tower-base pitching moments are not included here because the mean values

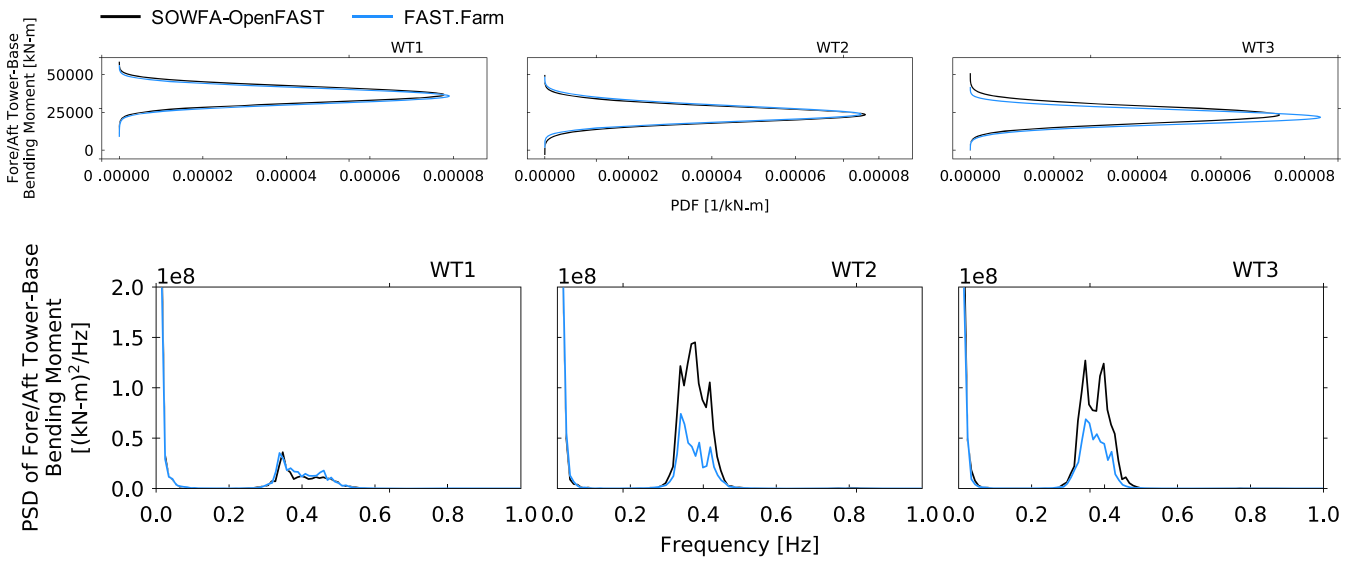
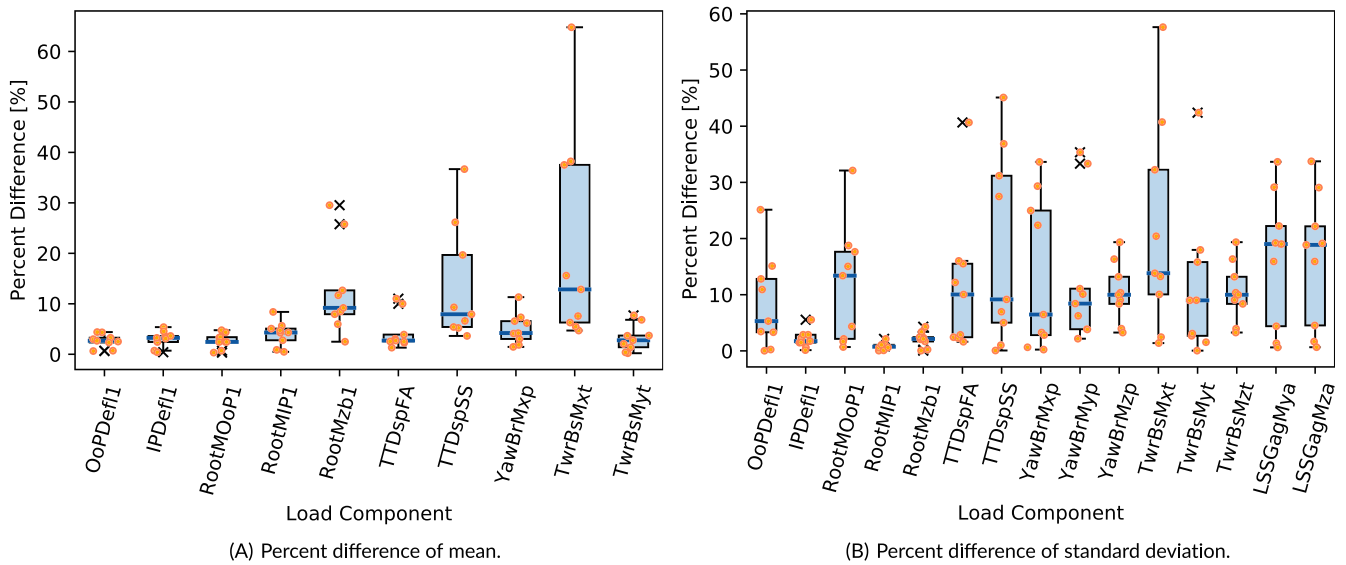
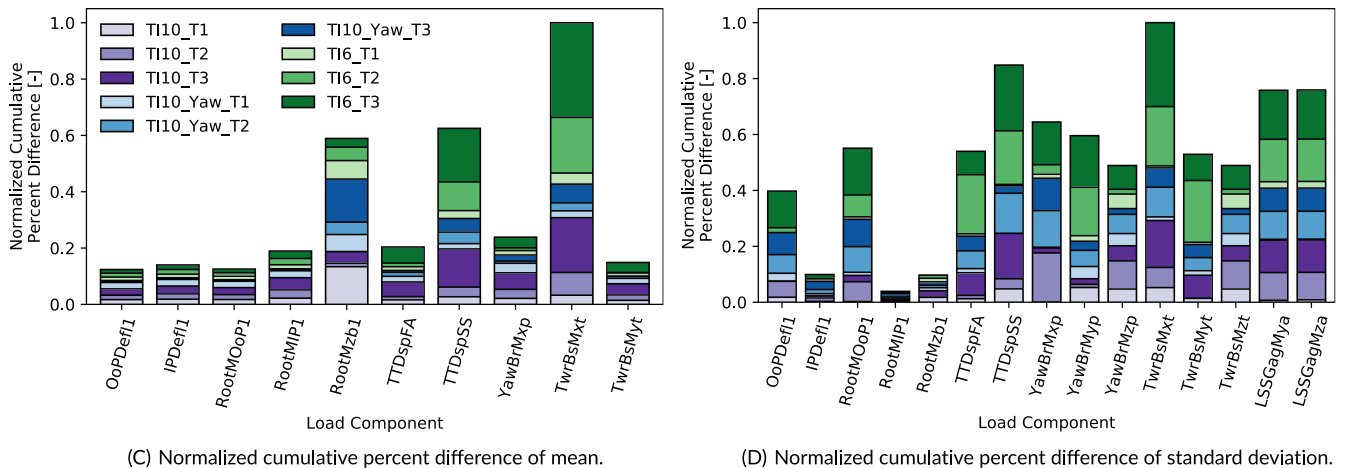


FIGURE 14 Probability density function and power spectral density of FA tower-base bending moment for the case with 8 m/s high-turbulence inflow (Case V8_T110) [Colour figure can be viewed at wileyonlinelibrary.com]



(A) Percent difference of mean.

(B) Percent difference of standard deviation.



(C) Normalized cumulative percent difference of mean.

(D) Normalized cumulative percent difference of standard deviation.

FIGURE 15 Box and whisker plots of percent difference and normalized cumulative percent difference comparison by structural component [Colour figure can be viewed at wileyonlinelibrary.com]

approach zero, artificially inflating the resulting percent difference. When comparing %D results sorted by load QoI, minor differences between SOWFA-OpenFAST and FAST.Farm results are seen in mean blade loads and deflections, with $\%D(\bar{x})$ values remaining below 5% (10% for blade pitching moment). $\%D(\bar{x})$ also remains below 5% for tower-top FA displacement and tower-top SS bending moment. Larger differences are seen between SOWFA-OpenFAST and FAST.Farm results for the remaining structural QoI $\%D(\bar{x})$ quantities. In particular, $\%D(\bar{x})$ is above 10% for tower-base FA bending moment. Note, however, that minimum $\%D(\bar{x})$ values for this QoI are as low as 4.7% and maximum $\%D(\bar{x})$ values are as high as 64.8%, highlighting the variability between turbine and case results. Overall, $\%D(\sigma)$ values show similar agreement between solutions than $\%D(\bar{x})$ values with a maximum $\%D(\sigma)$ of 59% and $\%D(\sigma)$ values remaining below 20%. There is considerably less spread in $\%D(\sigma)$ results compared with $\%D(\bar{x})$ results.

Comparisons between SOWFA-OpenFAST and FAST.Farm results are further investigated by showing the cumulative %D results for each structural QoI, normalized by the maximum cumulative %D value across all structural QoI (Equation 14), shown in Figure 15c,d.

$$\%D_{cumulative} = \frac{\sum \%D_i}{MAX(\%D)} \tag{14}$$

Here, each color group represents a different simulation case, and the color gradient shows the separate turbine results. Similar trends between loads are seen compared with Figure 15a,b. Here, however, it is clear that some cases or turbines result in higher %D results within a certain QoI. For example, $\%D(\sigma)$ values are overall much higher for Case V8_Tl6, again resulting from the importance of wake-added turbulence for low ambient Tl.

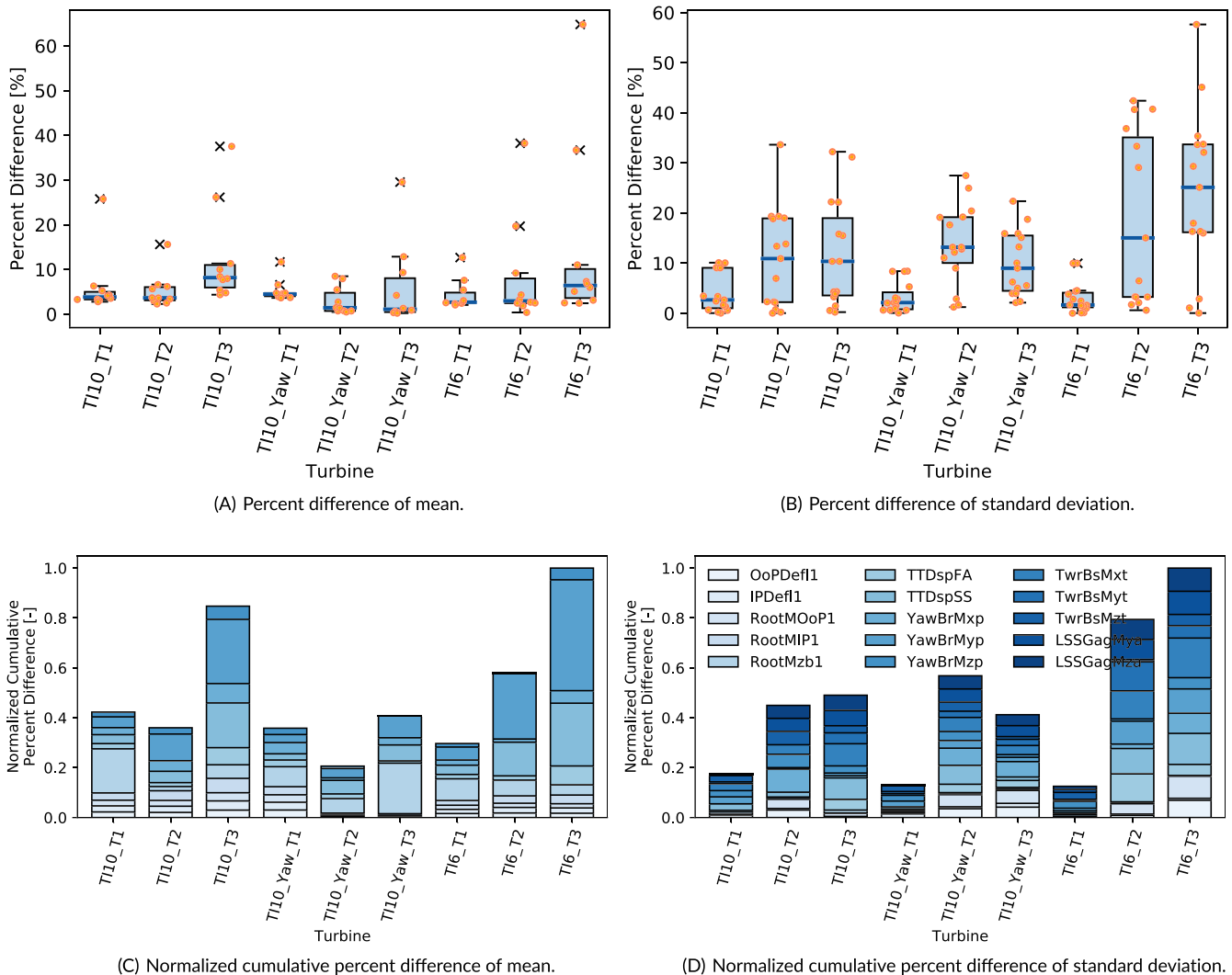


FIGURE 16 Box and whisker plots of percent difference and normalized cumulative percent difference comparison for all load channels by turbine and case [Colour figure can be viewed at wileyonlinelibrary.com]

To further expand on the differences associated with low ambient TI, the %D results from above are sorted by turbine and case, shown in Figure 16a, b. From this plot, it is seen that $\%D(\bar{x})$ values remain below 12%, and $\%D(\sigma)$ values remain below 26% for all turbines in all cases, yet maximum $\%D(\bar{x})$ and $\%D(\sigma)$ values can extend well above those values, as detailed above. This shows, however, that overall turbine structural response agrees very well between turbines and cases with a few structural QoIs resulting in higher differences. As before, cumulative %D results for each turbine and case, normalized by the maximum cumulative %D value across all turbines in all cases, are shown in Figure 16c,d. As expected, $\%D(\bar{x})$ and $\%D(\sigma)$ values are lower for WT1 than downstream turbines. $\%D(\bar{x})$ for WT3 are higher than WT2 for cases V8_TI10_Yaw and V8_TI6, with comparable levels between WT2 and WT3 for Case V8_TI10. When no turbines are yawed, $\%D(\sigma)$ values tend to be higher for WT3 than WT2. Most notably, there is a more drastic difference between WT1 $\%D(\sigma)$ values and downstream values, as compared with $\%D(\bar{x})$ values. This increased difference for downstream turbine results is likely due to the lack of wake-added turbulence in FAST.Farm simulations and more high-frequency wake content in LES.

4 | CONCLUSIONS

FAST.Farm is a new mid-fidelity engineering tool developed by the NREL targeted at accurately and efficiently predicting wind turbine power production and structural loading in wind farm settings, including wake interactions between turbines. FAST.Farm is based on some of the principles of the DWM model—including passive tracer modeling of wake meandering—but also addresses many of the limitations of previous DWM implementations.

The objective of this work is to quantify the ability of FAST.Farm to accurately predict turbine structural response in a small wind farm. This is done by comparing FAST.Farm structural response to coupled SOWFA-OpenFAST results for three laterally aligned turbines for differing atmospheric inflows. FAST.Farm and SOWFA-OpenFAST structural results are compared across 15 QoIs, including blade root moments, low-speed shaft moments, tower-top and tower-base moments, blade tip displacements, and tower-top displacements. For all considered structural components, strong agreement is seen between time series results for upstream turbines, with increased differences for downstream turbines. For statistical quantities, higher differences were seen for cases with lower ambient TI and yawed turbines due to the lack of wake-added turbulence and curled wake in FAST.Farm. However, the statistical quantities of the loads were in good agreement between the two simulation approaches, with average percent differences of mean and standard deviation for each QoI remaining below 20%. Statistical results compare well for turbine blade structural components in particular, with most average percent differences of the mean and standard deviation remaining below 5%. However, larger differences were seen for the tower-top and tower-base bending moments, related to more high-frequency energy content in the wake of LES. For some QoI, the percent difference of both the mean and standard deviation varied as much as 50%, depending on the turbine and case being considered, highlighting the variability between turbine and case results. Overall, flexible turbine structural results are comparable between FAST.Farm and SOWFA-OpenFAST simulations, especially for blade loads. These results establish confidence for applying FAST.Farm to wind farm power performance and loads analyses and identifying areas where further model validations and model improvements should be targeted.

ACKNOWLEDGEMENTS

This work was authored by Alliance for Sustainable Energy, LLC, the manager and operator of the National Renewable Energy Laboratory for the US Department of Energy (DOE) under contract no. DE-AC36-08GO28308. Funding is provided by the Department of Energy Office of Energy Efficiency and Renewable Energy, Wind Energy Technologies Office. The views expressed in the article do not necessarily represent the views of the DOE or the US Government. The US Government retains and the publisher, by accepting the article for publication, acknowledges that the US Government retains a nonexclusive, paid-up, irrevocable, worldwide license to publish or reproduce the published form of this work, or allow others to do so, for US Government purposes.

The research was performed using computational resources sponsored by the Department of Energy's Office of Energy Efficiency and Renewable Energy and located at the National Renewable Energy Laboratory.

The authors would like to thank Eliot Quon of NREL for his assistance with teaching the lead author how to run SOWFA and SOWFA-OpenFAST simulations.

PEER REVIEW

The peer review history for this article is available at <https://publons.com/publon/10.1002/we.2581>

ORCID

Kelsey Shaler  <https://orcid.org/0000-0002-7563-3377>

REFERENCES

1. Floris documentation. <https://floris.readthedocs.io/en/documentation/>; 2019.

2. Simley E, Fleming P, King J. Field validation of wake steering control with wind direction variability. *J Phys Conf Ser.* 2020;1452:12012.
3. Churchfield MJ, Moriarty PJ, Martinez LA, et al. A large-eddy simulation of wind-plant aerodynamics. In: 50th AIAA Aerospace Sciences Meeting. AIAA; 2012; Nashville, TN:537.
4. Jonkman J, Annoni J, Hayman G, Jonkman B, Purkayastha A. Development of fast.farm: a new multiphysics engineering tool for wind-farm design and analysis. In: 35th Wind Energy Symposium. AIAA; 2017; Grapevine, TX:454.
5. Jonkman J, Doubrawa P, Hamilton N, Annoni J, Fleming P. Validation of FAST.Farm against large-eddy simulations. *J Phys Conf Ser.* 2018;1037:1–13. <https://doi.org/10.1088/1742-6596/1037/6/062005>
6. Shaler K, Jonkman J, Doubrawa P, Hamilton N. Fast.farm response of varying wind inflow techniques. In 37th Wind Energy Symposium. San Diego, CA: AIAA; 2019:1–16.
7. Shaler K, Debnath M, Jonkman J. Validation of fast.farm against full-scale turbine SCADA data for a small wind farm. *J Phys Conf Ser.* 2020;1618: 62061.
8. Doubrawa P, Quon E, Martinez-Tossas LA, et al. Multimodel validation of single wakes in neutral and stratified atmospheric conditions. *Wind Energy.* 2020;23(11):2027–2055. <https://doi.org/10.1002/we.2543>
9. Wise A, Bachynski EE. Analysis of wake effects on global responses for a floating two-turbine case. *J Phys Conf Ser.* 2019;1356:12004.
10. Wise A, Bachynski EE. Wake meandering effects on floating wind turbines. *Wind Energy.* 2017;20:1083–1096.
11. Larsen GC, Madsen HA, Thomsen K, et al. Wake meander: a pragmatic approach. *Wind Energy.* 2008;11:337–95.
12. Jonkman J. The new modularization framework for the fast wind turbine CAE tool. In 51st AIAA Aerospace Sciences Meeting. Dallas, TX: AIAA; 2013:1–26.
13. Doubrawa P, Annoni J, Jonkman J, et al. Optimization-based calibration of FAST.Farm parameters against SOWFA. In 36th Wind Energy Symposium. Kissimmee, FL: AIAA; 2018:1–16.
14. Jonkman JM, Shaler K. Fast.farm user's guide and theory manual. NREL/TP-xxxxx, Golden, CO, National Renewable Energy Laboratory; 2020.
15. Ainslie JF. Calculating the flowfield in the wake of wind turbines. *J Wind Eng Indust Aerodyn.* 1988;27:213–224.
16. Crank J, Nicolson P. A practical method for numerical evaluation of solutions of partial differential equations of the heat-conduction type. *Adv Comput Math.* 1996;6:207–226.
17. Madsen HA, Larsen GC, Larsen TJ, Troldborg N, Mikkelsen R. Calibration and validation of the dynamic wake meandering model for implementation in an aeroelastic code. *J Solar Energy Eng.* 2010;132(4):1–14. <https://doi.org/10.1115/1.4002555>
18. Keck R-E, Veldkamp D, Wedel-Heinen JJ, Forsberg J. A consistent turbulence formulation for the dynamic wake meandering model in the atmospheric boundary layer. *Phd thesis:* DTU, Denmark; 2013.
19. Jonkman B. Turbsim user's guide v2.00.00. Tech. Rep. NREL/TP, Golden, CO, National Renewable Energy Laboratory; 2014.
20. Sowfa. Accessed: 2019-10-05.
21. Shaler K, Jonkman J, Hamilton N. Effects of inflow spatiotemporal discretization on wake meandering and turbine structural response using FAST.Farm. *J Phys Conf Ser.* 2019;1256:1–12. <https://doi.org/10.1088/1742-6596/1256/1/012023>
22. Katicc I, Hojstrup J, Jensen NO. A simple model for cluster efficiency. In: European Wind Energy Association Conference and Exhibition; 1986; Rome, Italy:407–410.

How to cite this article: Shaler K, Jonkman J. FAST.Farm development and validation of structural load prediction against large eddy simulations. *Wind Energy.* 2021;24:428–449. <https://doi.org/10.1002/we.2581>